JEM

Article

Mannose receptor high, M2 dermal macrophages mediate nonhealing *Leishmania major* infection in a Th1 immune environment

Sang Hun Lee,[1] Melanie Charmoy,[1] Audrey Romano,[1] Andrea Paun,[1] Mariana M. Chaves,[1] Frederick O. Cope,[2] David A. Ralph,[2] and David L. Sacks[1]

[1]Laboratory of Parasitic Diseases, National Institute of Allergy and Infectious Diseases, National Institutes of Health, Bethesda, MD
[2]Navidea Biopharmaceuticals, Dublin, OH

The origin and functional specialization of dermal macrophages in cutaneous infections have been little studied. In this paper, we show that a strain of *Leishmania major* (*L. major* Seidman [LmSd]) that produces nonhealing cutaneous lesions in conventionally resistant C57BL/6 mice was more efficiently taken up by M2-polarized bone marrow (BM)–derived macrophages (BMDMs) in vitro and by mannose receptor (MR)^{hi} dermal macrophages in vivo compared with a healing strain (*L. major* Friedlin V1). Both in steady and in T helper type 1 (Th1) cell–driven inflammatory states, the MR^{hi} dermal macrophages showed M2 characteristics. The dermal macrophages were radio resistant and not replaced by monocytes or adult BM-derived cells during infection, but were locally maintained by IL-4 and IL-10. Notably, the favored infection of M2 BMDMs by LmSd in vitro was MR dependent, and genetic deletion of MR or selective depletion of MR^{hi} dermal macrophages by anti–CSF-1 receptor antibody reversed the nonhealing phenotype. We conclude that embryonic-derived, MR^{hi} dermal macrophages are permissive for parasite growth even in a strong Th1-immune environment, and the preferential infection of these cells plays a crucial role in the severity of cutaneous disease.

The Journal of Experimental Medicine

INTRODUCTION

The control of intracellular pathogens such as *Leishmania major* can be understood in the context of macrophages found in two broadly distinctive activation states, termed M1 and M2 (Gordon, 2003). M1 macrophages are induced by IFN-γ and microbial stimuli and have enhanced antimicrobial capacity, whereas M2 macrophages are permissive to intracellular microbial growth but can mediate type 2 immunity against helminth infection, as well as contribute to tissue repair. Recent studies have emphasized the plasticity of tissue macrophages with regard to their activation states and have suggested that their ontogeny and tissue-derived signals shape their functional specialization (Gautier et al., 2012; Lavin et al., 2014). As most studies have focused on steady-state conditions or sterile tissue injury, the question of whether tissue macrophages can be reprogrammed in infection-driven inflammatory settings has only rarely been addressed. Recently, in a sequential infection model involving nematodes and bacteria, reprogramming of the peritoneum-resident macrophage appeared limited compared with newly recruited monocyte-derived macrophages, suggesting that the origin of macrophages plays an important role in their functional adaptation (Rückerl et al., 2017). Little is known regarding the plasticity of dermis-resident macrophages and their relative contributions to antimicrobial immunity or to pathology in cutaneous infection.

We have described a model of nonhealing cutaneous leishmaniasis in C57BL/6 mice infected with the *L. major* Seidman (LmSd) strain that was isolated from a patient with nonhealing cutaneous lesions (Anderson et al., 2005). Paradoxically, the nonhealing cutaneous infections occur within a strong T helper type 1 (Th1) cell setting that reflects the immunological conditions associated with many chronic forms of cutaneous leishmaniasis in humans (Pirmez et al., 1993; Louzir et al., 1998). Multiple factors, including IL-10, IL-1β, and inflammasome activation, contribute to the pathogenesis of nonhealing infection with LmSd (Anderson et al., 2005; Charmoy et al., 2016). To date, however, it has not been possible to explain how these factors act in concert to promote a nonhealing phenotype in such a strong Th1 environment.

In the experiments reported here, we have identified a population of M2-like dermal macrophages that are present under steady-state conditions and that are preferentially infected by the LmSd strain in a mannose receptor (MR)–dependent fashion to promote nonhealing cutaneous disease. The dermal macrophages are not replaced by blood precursors during infection, but are locally maintained by IL-4 and IL-10 and retain M2 functionality despite the high levels of IFN-γ produced in the site. So far as we are aware, this is

Correspondence to David L. Sacks: dsacks@niaid.nih.gov

The Rockefeller University Press
J. Exp. Med. 2018 Vol. 215 No. 1 357–375
https://doi.org/10.1084/jem.20171389

the first demonstration that the severity of cutaneous infection can be linked to the preferential targeting of dermis-resident macrophages.

RESULTS

MR mediates preferential uptake of nonhealing *L. major* strains by bone marrow (BM)–derived macrophages (BMDMs) in vitro

As previously described (Charmoy et al., 2016), infection of C57BL/6 mice with a low dose of 1,000 LmSd metacyclic promastigotes results in a nonhealing lesion that eventually ulcerates, leading to complete erosion of the ear dermis (Fig. S1). In contrast, the *L. major* Friedlin V1 (LmFn) strain produces a chronic, nonulcerative, nodular lesion that eventually heals. To determine whether the differences in clinical outcome might be reflected in their interactions with innate cells, the *L. major* strains were compared for infection and replication in M-CSF–induced BMDMs in vitro (Fig. 1 A). Metacyclic promastigotes of LmSd showed an approximately twofold higher infection than LmFn at 5 h postinfection (p.i.), which was maintained during 3 d of culture. When calculated as the mean number of parasites per infected cell, LmSd and LmFn replicated similarly. The amastigote stage of LmSd was also more efficiently taken up than LmFn amastigotes and with a more rapid kinetic compared with metacyclic promastigotes of either strain (Fig. 1 B). Their intracellular replication rates were again similar. The association between the differences in *L. major* uptake by BMDMs in vitro and the infection outcomes in vivo was reinforced by the analysis of a series of genetic hybrids (LmFnSd) generated from sexual crosses between LmFn and LmSd (Inbar et al., 2013). The progeny clones inherited either the healing or nonhealing parental phenotypes (Fig. 1, C and D), and there was a precise correlation of the nonhealing hybrids with their more efficient uptake by BMDMs (Fig. 1 E).

Various receptors can mediate phagocytosis of promastigotes and amastigotes by macrophages, including MR, fibronectin receptor, or complement receptor 3 (CR3; Ueno and Wilson, 2012). To address the possible role of either MR or fibronectin receptor in the increased infection by LmSd, we treated the BMDMs with BSA-mannose or RGDS (H-Arg-Gly-Asp-Ser-OH tetrapeptide found on the integrin-binding domain of fibronectin), respectively, before infection. Using metacyclic promastigotes, we observed a dose-dependent reduction of LmSd infection in BMDMs treated with BSA-mannose, whereas no effect on infection by LmFn was observed (Fig. 1 F). There was no effect of RGDS treatment on either strain. The inhibition of LmSd infection in BSA-mannose–treated BMDMs was also observed using amastigotes (Fig. 1 G). CR3- and C3-deficient BMDMs showed no reduction, but rather a slight increase in the favored uptake of both LmFn and LmSd, which maintained a twofold difference between strains (Fig. 1 H). Finally, LmSd uptake by BMDMs from MR-deficient mice (*mrc1*$^{-/-}$) was significantly reduced, whereas uptake of LmFn was not affected (Fig. 1 I).

MR is well described as a marker of M2 macrophages (Murray, 2017). M-CSF–differentiated BMDMs expressed higher levels of MR in comparison to GM-CSF–induced BM dendritic cells (DCs; Fig. 1 J). Subsequent treatment with M1 stimuli (LPS or IFN-γ plus LPS) decreased MR expression in BMDMs, whereas treatment with IL-10, and especially with IL-4 plus IL-10, though not with IL-4 and/or IL-13 alone, enhanced MR expression (Fig. 1 K). Accordingly, the favored uptake of LmSd versus LmFn was lost when BMDMs were converted to M1 macrophages, and both strains were killed after 3 d of infection (Fig. 1 L). In contrast, stronger M2 polarization after stimulation with IL-4/-10 resulted in a pronounced difference in infection by LmSd versus LmFn, whereas both strains survived and replicated in these cells. Collectively, these results indicate that the higher infectivity of LmSd is caused by an MR-dependent uptake of parasites that promotes preferential infection of M2 BMDMs in vitro.

Identification and functional characterization of MR^{hi} macrophages in the steady-state dermis

To identify cells expressing MR in the skin, we analyzed ear cells from naive mice (Fig. 2 A). Staining for Ly6C versus MR on CD11b^{+} cells that were negative for several lineage markers identified four distinct populations, designated P1–P4. High expression of MR was confined to the P4 population defined as Ly6C^{int}MR^{hi}, which comprises 30% of CD11b^{+} cells in the steady-state skin (Fig. 2, A and B). The P4 population was selectively labeled in vivo by a fluorescent reagent (Manocept–Alexa Fluor 488) containing mannose moieties (Fig. 2 C and Fig. S2, A and B; Azad et al., 2015). Applying an additional set of markers recently used to define subsets of myeloid cells present in the steady-state ear dermis (Tamoutounour et al., 2013), the P4 cells were CD64^{+}CCR2^{low}, identifying the population as dermal macrophages, of which 95% were MHCII^{-} (Fig. S2 C). Applying these additional markers to cells within the P1–P3 gates identified the populations as inflammatory monocytes (P1), monocyte-derived DCS (moDCs; P2), and moDCs plus CD11b^{+}Ly6C^{-}CD64^{-} dermal DCs (P3). P1 cells displayed morphological features of monocytes, whereas P2 and P3 populations showed a phagocyte morphology with larger cytoplasm and small processes, and P4 cells showed characteristics of mature macrophages with abundant cytoplasmic vacuoles and melanin granules (Fig. 2 D).

In addition to MR, several other previously described M2 markers (Hughes et al., 2008; Shaul et al., 2010; Huang et al., 2014; Thornley et al., 2014; Zagórska et al., 2014; Murray, 2017) were highly expressed in P4 recovered from the steady-state dermis, including CD36 (fatty acid translocase), CD209 (DC-SIGN), Colec12 (scavenger receptor), CD301 (CLEC10A, C-type lectin), MERTK (TAM receptor tyrosine kinase), Tim-4 (PtdSer recognition receptor), Tgfr2 (TGF-β receptor 2), Lyve-1 (angiogenic factor), and S1pr1 (Sphingosine-1-phosphate receptor 1; Fig. 2 E and Fig. S2 D). Of these, only Lyve-1 and S1pr1 were elevated in P1,

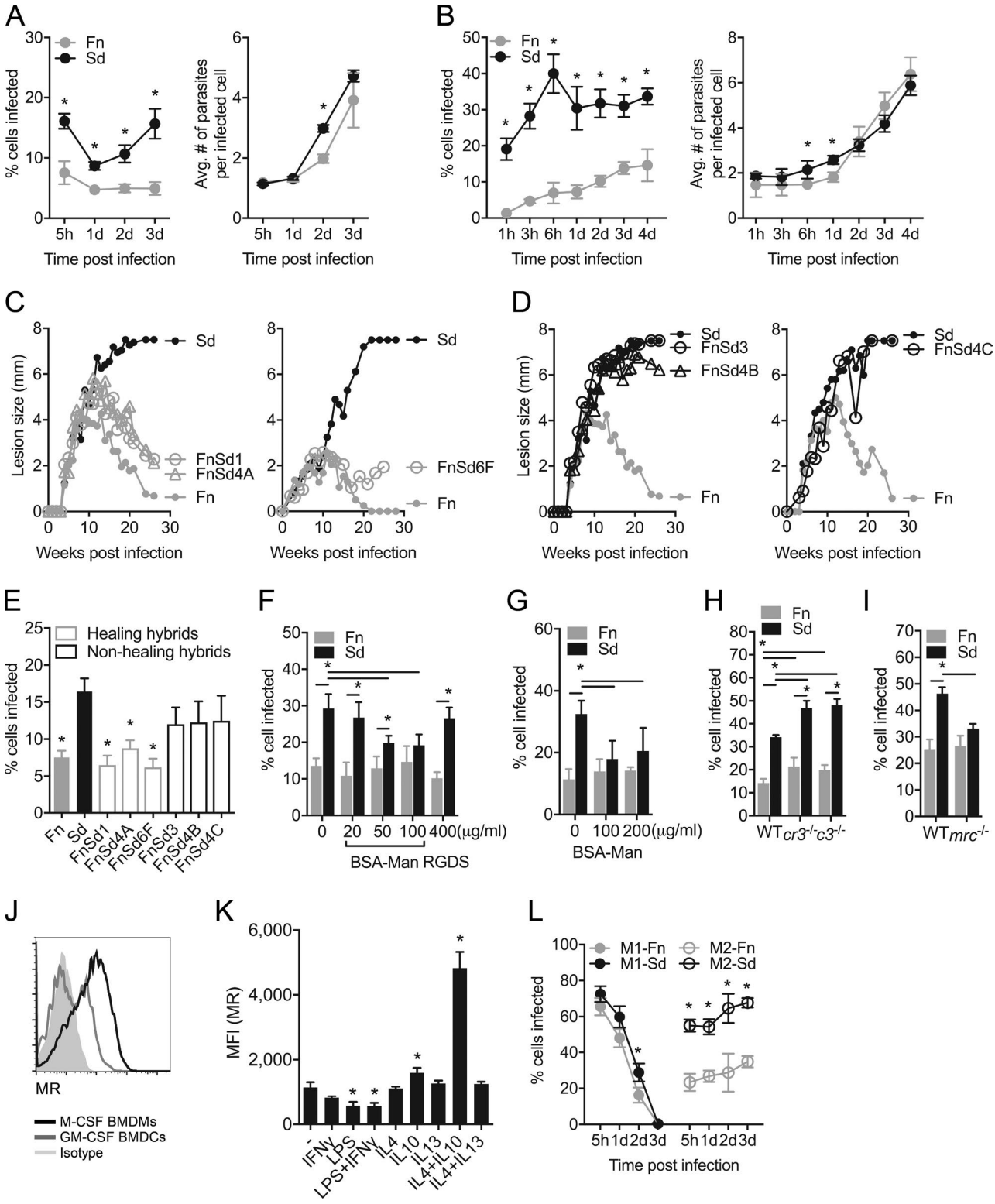

Figure 1. **The MR mediates preferential uptake of nonhealing *L. major* strains by BMDMs in vitro. (A)** BMDMs from C57BL/6 mice were infected with metacyclic promastigotes at an MOI of 4 for 5 h, washed three times, and incubated for 1, 2, and 3 d. Giemsa-stained cells were scored for the percentage of total cells infected and the mean number of parasites per infected cell at each time point. **(B)** BMDMs were infected with amastigotes at an MOI of 1 for 1, 3, and 6 h, washed three times, and incubated for 1, 2, 3, and 4 d. (A and B) $n = 4$; data representative of three independent experiments. **(C and D)** Development of nodular lesions over the course of infection with 10^3 metacyclic promastigotes of the parental clones (Sd and Fn) and their genetic

and none were elevated in P2 or P3. Because the high expression of MERTK and Tim-4 suggested a role in apoptotic cell clearance, this function was compared after intradermal injection of CFSE-labeled apoptotic thymocytes. Most apoptotic cells were captured by P4 dermal macrophages within 10 min, whereas P1–P3 and CD11b$^+$Ly6C$^-$CD64$^-$ dermal DCs showed delayed uptake (Fig. 2 F). Recently, a subset of skin-resident macrophages was shown to continuously capture blood-borne macromolecules using protrusions across the endothelial junctions (Barreiro et al., 2016). We investigated the ability of P4 to phagocytose high–molecular weight FITC-dextran from the blood vessel lumen. Only the P4 dermal macrophages were able to rapidly capture the FITC-dextran (Fig. 2 G). P4 cells were also rapidly (within 3 min) and selectively labeled by intravenously injected anti-MR antibody (Fig. 2 H). Together, the results suggest that the P4 cells show M2-like phenotypes, highly phagocytic/trans-endothelial capability, and homeostatic functions related to the rapid clearance of apoptotic cells.

P4 dermal macrophages are not replaced by blood precursors during infection

After infection, the recruitment of monocytes was accompanied by increased numbers of other infiltrating cells, including eosinophils, natural killer cells, and T cells (Fig. 3, A and B). However, the number of P4 dermis-resident macrophages showed only a slight increase, suggesting that monocytes were not likely to differentiate into P4 during infection. To better address the ontogeny of P4 during infection, we infected *cx3cr1-gfp* mice with LmSd to track cells originating from GFP$^+$ monocytes (Fig. 3 C). In contrast to P1–P3, for which 40–80% of the cells were GFP$^+$ within the first week of infection, <10% of P4 was GFP$^+$. Consistent with these results, we observed the differentiation of adoptively transferred CD45.1$^+$GFP$^+$ monocytes into P2 and P3 moDCs, but not to P4 dermal macrophages in CD45.2$^+$ recipient mice infected with LmSd (Fig. 3 D). The fact that 40% of adoptively transferred GFP$^+$ monocytes lost their GFP expression during their differentiation to moDCs explains why only 40–80% of P1–P3 were GFP$^+$ in the *cx3cr1-gfp* mice (Fig. 3, C and D). Using BM chimeras, >90% of P4 remained of recipient origin in naive mice, even at 1 mo after BM transfer, whereas the other myeloid populations in the skin were >75% donor derived (Fig. 3 E). Moreover, P4 remained almost entirely of recipient origin during LmSd infection in these BM chimeras. Finally, we established parabionts between CD45.1$^+$ and CD45.2$^+$ congenic mice that were infected with LmSd, one ear in each partner, after 2 wk when their shared blood supply had been established (Fig. 3 F). After 2 wk of infection, all of the lymphoid and myeloid cells recovered from the ear dermis, with the exception of P4, showed exchange between partners, with 20–50% originating from the parabiotic partner. The P4 dermal macrophages were entirely maintained without input from blood precursors originating in the parabiotic partner. Together, these data strongly indicate that MR^{hi} dermal macrophages represent a radio-resistant population that is not replaced by adult BM–derived progenitors during infection.

Preferential infection of P4 dermal macrophages by LmSd in vivo

Intracellular amastigotes were readily observed in sorted populations of P1–P4 cells recovered from RFP$^+$ LmSd-infected ears (Fig. 4 A). In immunostained vertical sections of the ear dermis infected with LmSd-RFP (Fig. 4 B), we found MR$^+$ cells containing melanin granules (Fig. 4 B, insets 3 and 6) in both the dorsal and ventral aspects of the ear pinnae. MR$^+$ cells harboring RFP$^+$ parasites were observed in inflamed regions of the section (Fig. 4 B, insets 1, 4, and 5) in contrast to the noninflamed periphery (Fig. 4 B, inset 2).

To determine whether the MR^{hi} dermal macrophages were preferentially infected by LmSd, as would be predicted based on the in vitro findings involving BMDMs, we measured the frequencies of CD11b$^+$ dermal populations and their relative levels of parasitization by LmSd-RFP and LmFn-RFP during the early stage of infection. The percentages of each myeloid population were comparable between these strains, with P3 being the predominant population at days 2 and 5 and increased frequencies of P1 monocytes and eosinophils by day 12 p.i. (Fig. 4 C). P4 was the predominant subset infected by LmSd, and it was the only population showing a significant difference in infection between the strains

hybrids (FnSd1, FnSd4A, FnSd6F, FnSd3, FnSd4B, and FnSd4C; $n = 8$; data representative of two independent experiments). **(E)** BMDMs were infected with metacyclic promastigotes of the parental and hybrid clones at an MOI of 4 for 5 h. Giemsa-stained cells were scored for the percentage of total cells infected ($n = 4$; data representative of two independent experiments). **(F)** BMDMs were pretreated with BSA-mannose or RGDS for 5 h and infected with metacyclic promastigotes at an MOI of 4 for 5 h ($n = 4$; data representative of three independent experiments). **(G)** BMDMs were pretreated with BSA-mannose for 5 h and infected with amastigotes at an MOI of 1 for 3 h ($n = 4$; data representative of two independent experiments). **(H and I)** BMDMs from WT, *cr3*$^{-/-}$, and *c3*$^{-/-}$ mice (H) or from WT and *mrc*$^{-/-}$ mice (I) were infected with metacyclic promastigotes at an MOI of 4 for 5 h ($n = 4$; data representative of two independent experiments). Giemsa-stained cells were scored for the percentage of total of cells infected. **(J)** MR expression on M-CSF–induced BMDMs or GM-CSF–induced BMDCs (data representative of two independent experiments). **(K)** MR expression on BMDMs treated with 50 ng/ml IFN-γ, 10 ng/ml LPS, 10 ng/ml IL-4, 10 ng/ml IL-10, 10 ng/ml IL-13, or combinations for 48 h ($n = 6$; data representative of two independent experiments). **(L)** Giemsa-stained BMDMs were scored for the percentage of total cells infected that were prestimulated with either 10 ng/ml LPS and 50 ng/ml IFN-γ (M1) or 10 ng/ml IL-4 and 10 ng/ml IL-10 (M2) for 24 h, followed by infection with metacyclic promastigotes at an MOI of 4 for 5 h, and incubated for 1, 2, and 3 d ($n = 4$; data representative of two independent experiments). Values represent mean ± standard deviation. *, $P < 0.05$ by nonparametric Mann-Whitney test (A, B, F–I, and L) and by one-way ANOVA with Dunn's posttest compared with LmSd (E) or with nontreated WT (K).

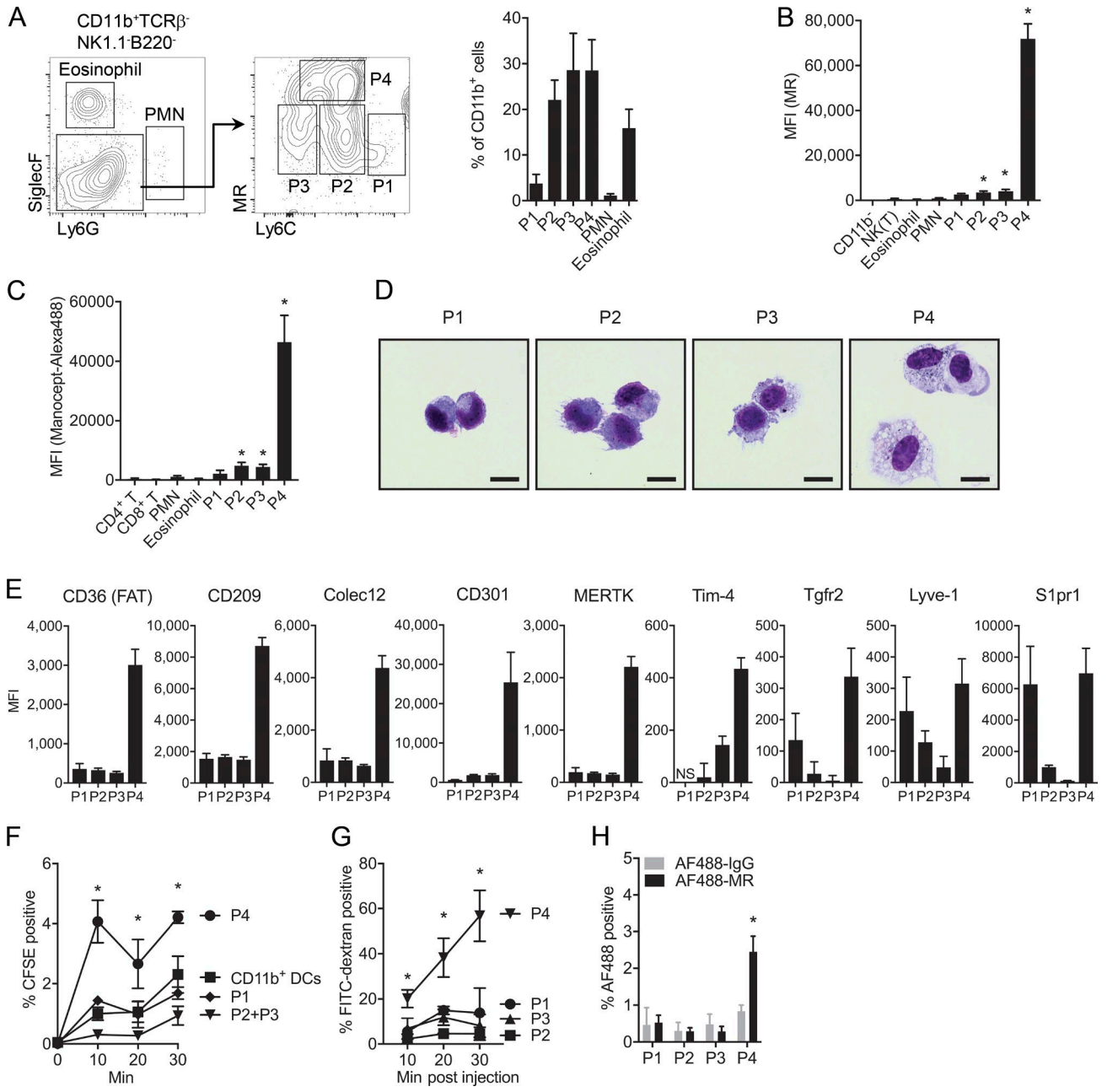

Figure 2. **MR identifies a population of highly phagocytic M2 macrophages in the steady-state dermis. (A)** Representative flow cytometric analysis of ear isolates prepared from naive mice. $CD11b^+Ly6G^-SiglecF^-$-gated cells were analyzed for the expression of Ly6C and MR and subdivided into a $Ly6C^{hi}MR^{lo}$ (P1), $Ly6C^{int}MR^{lo}$ (P2), $Ly6C^{lo}MR^{lo}$ (P3), and $Ly6C^{int}MR^{hi}$ (P4). Bar graph shows the frequencies of the myeloid subsets identified. **(B)** Mean fluorescence index (MFI) for MR expression on indicated populations isolated from naive ears. (A and B) $n = 6$; data representative of three independent experiments. **(C)** MFIs of the labeled populations were quantified at 1 h after intravenous injection of 5 µg Manocept–Alexa Fluor 488 ($n = 6$; data representative of two independent experiments). PMN, polymorphonuclear leukocyte. **(D)** Light micrographs of Wright-Giemsa–stained P1–P4 populations sorted from naive ear. Bars, 10 µm (data representative of more than five independent experiments). **(E)** MFIs for selected M2 macrophage markers expressed on P1–P4 populations from naive ear. Background MFIs of isotype controls were subtracted (n = 6; data representative of two independent experiments; negative values are not depicted). **(F)** Uptake of apoptotic thymocytes by indicated populations of myeloid cells. Mice were injected in the ear dermis with 10^6 CFSE-labeled apoptotic thymocytes and sacrificed at 10–30 min for flow cytometric analysis of CFSE labeling in the ear dermal cells ($n = 4$; data representative of three independent experiments). **(G and H)** Flow cytometric analysis of the uptake of intraluminal dextran or anti-MR antibodies after intravenous injection with 2 MD FITC-dextran or Alexa Fluor 488–anti-MR antibodies (H) and sacrificed at 10–30 min or 3 min, respectively ($n = 4$; data representative of two independent experiments). Values represent mean ± standard deviation. *, $P < 0.05$ by one-way ANOVA with Dunn's posttest (B, C, F, and G) and by nonparametric Mann-Whitney test (H).

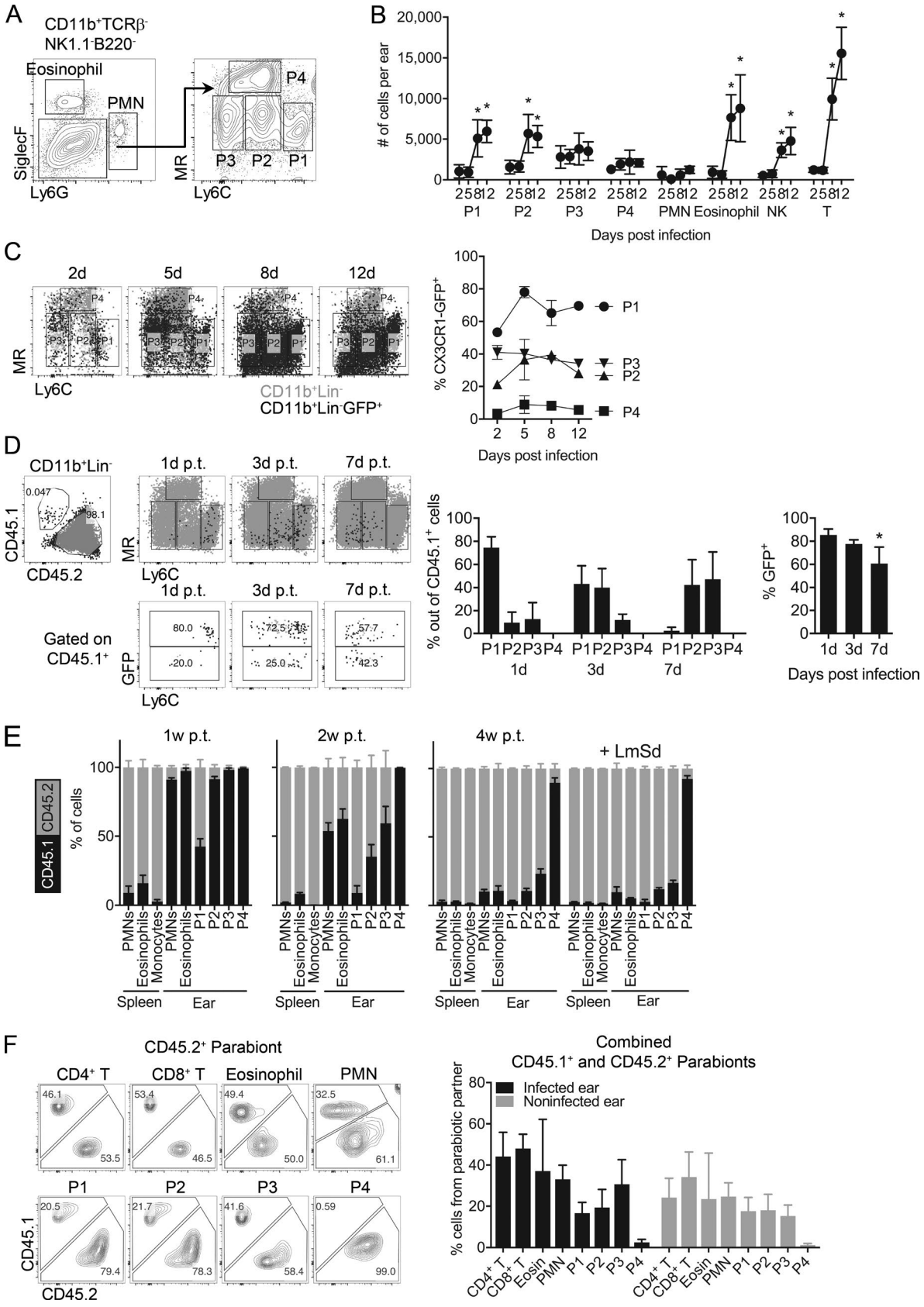
A
CD11b+TCRβ-
NK1.1-B220-
Eosinophil
PMN
SiglecF
Ly6G
MR
Ly6C
P4
P3
P2
P1
B
# of cells per ear
20,000
15,000
10,000
5,000
0
25812
P1
P2
P3
P4
PMN
Eosinophil
NK
T
Days post infection
C
2d
5d
8d
12d
MR
Ly6C
CD11b+Lin-
CD11b+Lin-GFP+
% CX3CR1-GFP+
100
80
60
40
20
0
2
5
8
12
Days post infection
D
CD11b+Lin-
1d p.t.
3d p.t.
7d p.t.
0.047
98.1
CD45.1
CD45.2
MR
Ly6C
Gated on
CD45.1+
GFP
80.0
20.0
72.5
25.0
57.7
42.3
% out of CD45.1+ cells
P1P2P3P4
1d
3d
7d
% GFP+
1d 3d 7d
Days post infection
E
1w p.t.
2w p.t.
4w p.t.
+ LmSd
CD45.1 CD45.2
% of cells
100
50
0
PMNs
Eosinophils
Monocytes
P1
P2
P3
P4
Spleen
Ear
F
CD45.2+ Parabiont
CD4+ T
CD8+ T
Eosinophil
PMN
46.1
53.5
53.4
46.5
49.4
50.0
32.5
61.1
P1
P2
P3
P4
20.5
79.4
21.7
78.3
41.6
58.4
0.59
99.0
CD45.1
CD45.2
Combined
CD45.1+ and CD45.2+ Parabionts
Infected ear
Noninfected ear
% cells from parabiotic partner
80
60
40
20
0
CD4+ T
CD8+ T
Eosin
PMN
P1
P2
P3
P4

(Fig. 4 D) at days 2 and 5 p.i. when there was no difference in overall parasite burden (Fig. 4 E). After 12 d of infection, P1/P3, as well as P4, showed increased infection by LmSd that was associated with a 10-fold increase in parasite burden compared with LmFn (Fig. 4, D and E). At later time points, when the respective healing and nonhealing outcomes were well established (Fig. 4 F), a high percentage of P4 was infected with LmSd, although the P1–P3 populations were also well parasitized during the chronic stage (Fig. 4 G).

Nonhealing infection with LmSd is MR dependent

The nonconsequential role of MR in *L. major* infection involving a healing strain (LmFn) has been previously reported (Akilov et al., 2007). To evaluate the role of MR in the nonhealing response to LmSd, we infected MR-deficient mice and measured lesion development and parasite burdens. The *mrc1*$^{-/-}$ mice were as resistant to LmSd infection as the WT mice infected with LmFn with respect to lesion size, pathology score, and parasite load (Fig. 5, A and B). Infected in parallel were *casp1/11*$^{-/-}$ and *il1r*$^{-/-}$ mice that displayed the healing phenotypes previously described (Charmoy et al., 2016).

P2 and P3 expressed low but significant levels of surface MR (Fig. 2 B) and bound low but significant amounts of Manocept–Alexa Fluor 488 (Fig. 2 C and Fig. S2, A and B). To address the possible role of these populations in the MR-dependent, nonhealing outcome, we generated BM chimeras between CD45.1$^+$ WT and CD45.2$^+$ *mrc*$^{-/-}$ animals, taking advantage of the fact that P4 is the only radio-resistant population of MR-expressing cells in the skin (Fig. 3 E). We used the MR-independent gating strategy for identification of CD11b$^+$Lin$^-$CCR2^{lo}CD64^{hi}Ly6C^{int} dermal macrophages (Tamoutounour et al., 2013) to determine chimerism in these BM chimeras (Fig. S2 C). At 16 wk after irradiation and 12 wk p.i. in the CD45.2$^+$ *mrc*$^{-/-}$ BM→CD45.1$^+$ WT chimeras, most of the myeloid and lymphoid populations recovered from the inoculation site had been completely replaced by BM-derived cells of donor origin. The exceptions were the T cells and the P4 dermal macrophages that remained of 25 and 75% recipient origin, respectively (Fig. 5 C). Confining MR expression to these cells was sufficient to promote the nonhealing outcome (Fig. 5, D and E). In contrast, in the WT BM→*mrc*$^{-/-}$ chimeras, only the dermal macrophages remained of predominant recipient origin (75%), and confining the absence of MR to these cells was sufficient to reproduce the resistance phenotype observed in the *mrc*$^{-/-}$ mice. Thus, MR expression on dermal macrophages is both necessary and sufficient for the evolution of the nonhealing infection.

The selective depletion of dermal macrophages ameliorates nonhealing infection with LmSd

M-CSF and CSF-1 receptor (CSF-1R) signaling are required for dermal macrophage development (Ginhoux and Jung, 2014). As blockade of the CSF-1R has been reported to deplete resident macrophages in various tissues, including skin (MacDonald et al., 2010), we attempted to selectively deplete the P4 population using an antibody against mouse CSF-1R (M279). The M279 treatment increased circulating M-CSF levels caused by blocking receptor-mediated consumption (Fig. S3 A). We also observed an accelerated weight gain relative to controls, as previously reported (Fig. S3 B; Sauter et al., 2014). Before infection, 3-wk-long M279 treatment resulted in a virtually complete depletion of P4, indicating that M-CSF plays a critical role in maintaining the steady-state levels of these cells (Fig. 6 A). Although an approximate twofold reduction in each of the other dermal myeloid populations was also observed in the M279-treated naive mice, their numbers were rapidly reconstituted after infection, likely the result of infiltration by unaffected blood-derived cells (Fig. 6 B and Fig. S3 C). At 9 d p.i., only the P4 population remained depleted in the infected skin. The selective effect on P4 appears to depend on the differential requirement for M-CSF to maintain this population rather than differential receptor expression because other myeloid cells also express CSF-1R (Fig. S3 D). Finally, M279-treated animals were able to control their infections with LmSd and were as resistant as controls infected with LmFn with respect to lesion size, pathology score, and parasite load (Fig. 6, C and D).

Figure 3. **P4 dermal macrophages do not originate from blood precursors. (A)** Representative flow cytometric analysis of ear isolates prepared from day 12–infected ears after infection with 2 × 10^5 LmSd (data representative of three independent experiments). **(B)** The total numbers of the indicated populations of the dermal cells in WT mice infected with 2 × 10^5 LmSd metacyclics (n = 6; data representative of three independent experiments). **(C)** Representative dot plots of GFP$^+$ cells within each of the P1–P4 populations in *cx3cr1-gfp* mice infected with 2 × 10^5 LmSd metacyclics for 2, 5, 8, and 12 d. The graph shows the percentage of each population, P1–P4, that was CXCR1-GFP$^+$. **(D)** CD45.1$^+$GFP$^+$ monocytes were sorted from BM cells of *cx3cr1-gfp* mice and adoptively transferred into CD45.2$^+$ C57BL/6 mice infected for 7 d with 2 × 10^5 LmSd. Representative dot plots showing adoptively transferred CD45.1$^+$GFP$^+$ monocytes (black) overlaid onto the P1–P4 populations (gray) and the GFP expression on the CD45.1$^+$ cells recovered from the ear dermis at different times after adoptive transfer. Bar graphs show the percentage of the total CD45.1$^+$ cells found in each population and the percentage of the total CD45.1$^+$ cells that remained GFP$^+$. p.t., post transfer. **(E)** The ratio between cells of donor origin (CD45.2, gray bars) and recipient origin (CD45.1, black bars) from ear isolates of BM chimeras at 1, 2, and 4 wk after BM transfer. A group of mice were infected with 2 × 10^5 LmSd at 2 wk after BM transfer and analyzed after another 2 wk. **(F)** Representative dot plots and bar graph showing the percentages of chimerism in the indicated populations present in the noninfected or infected ears of parabiotic mice for 12 d with 2 × 10^5 LmSd. (C–F) n = 4; data representative of two independent experiments. PMN, polymorphonuclear leukocyte. Values represent mean ± standard deviation. *, P < 0.05 by one-way ANOVA with Dunn's posttest compared with day 2 p.i. (B) and day 1 after transfer (D).

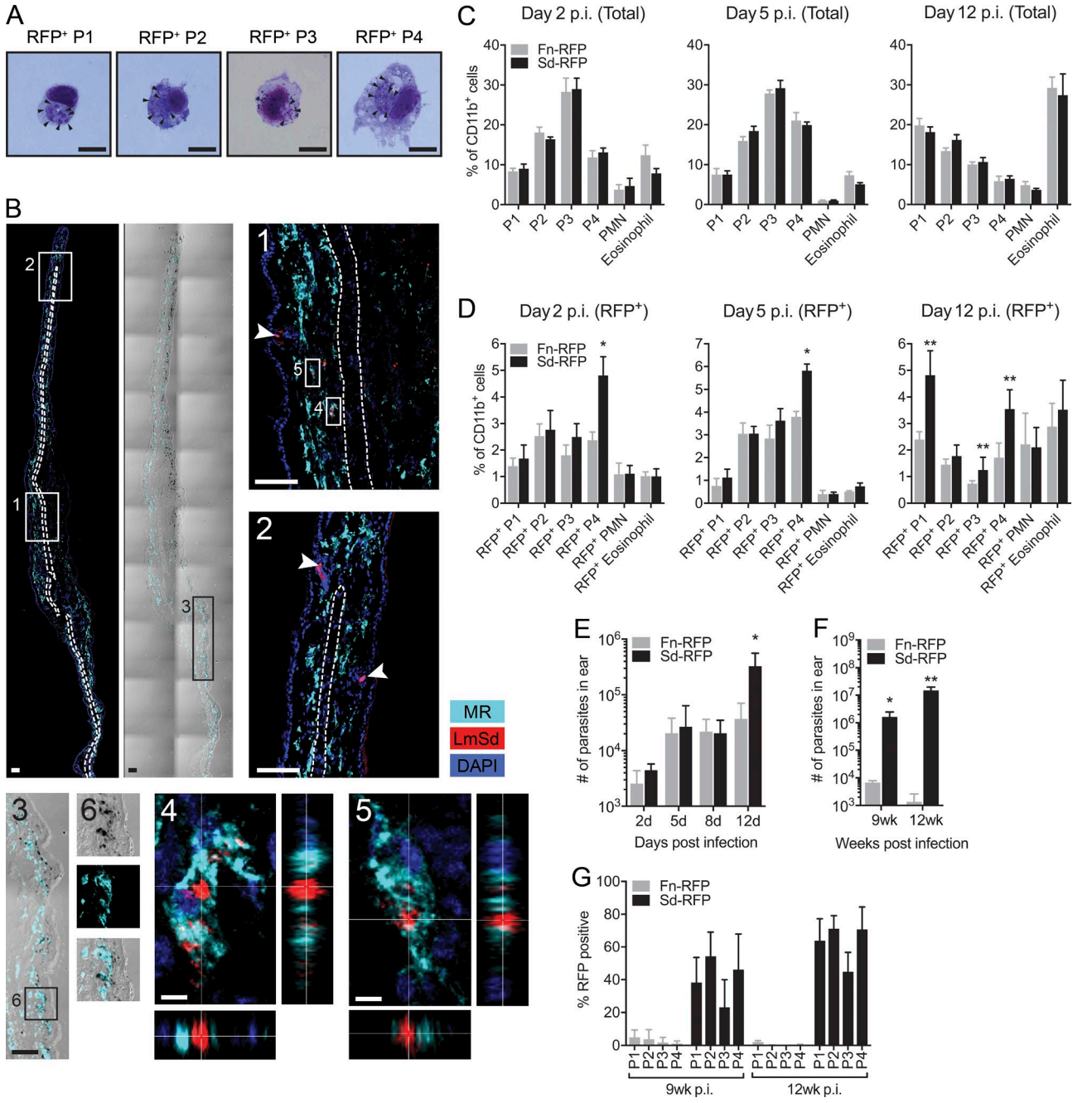

Figure 4. **LmSd selectively infects P4 dermal macrophages. (A)** Light microscopic appearance of Wright-Giemsa–stained P1–P4 populations sorted from infected ears. Arrowheads indicate amastigotes (data representative of more than five independent experiments). **(B)** Immunofluorescence staining and confocal microscopy on vertical sections of an infected ear showing LmSd-RFP (red), MR (cyan), and Hoechst 33342 (blue). Insets 1–6 show boxed areas at higher magnification. Dashed lines depict auricular cartilage. Thin white lines in insets 4 and 5 indicate corresponding points in the orthogonal planes, showing localization of RFP^+ parasites within the MR^+ cell. Arrowheads indicate hair follicles (data representative of two independent experiments). **(C–E)** Percentages of total (C) or RFP^+-infected (D) myeloid populations recovered from the ear at 2, 5, and 12 d p.i. with 2×10^5 RFP^+ LmSd and LmFn and parasite loads per infected ear (E). **(F and G)** Parasite loads per infected ear (F) and percentages of RFP^+-infected populations, P1–P4 (G), recovered from the ear at 9 and 12 wk p.i. with 10^3 RFP^+ LmSd and LmFn. (C–F) $n = 6$; data representative of two independent experiments. Values represent mean ± standard deviation. *, $P < 0.05$; **, $P \leq 0.01$ by nonparametric Mann-Whitney test (D and E). Bars: (A) 10 µm; (B) 100 µm; (except insets 4 and 5) 5 µm.

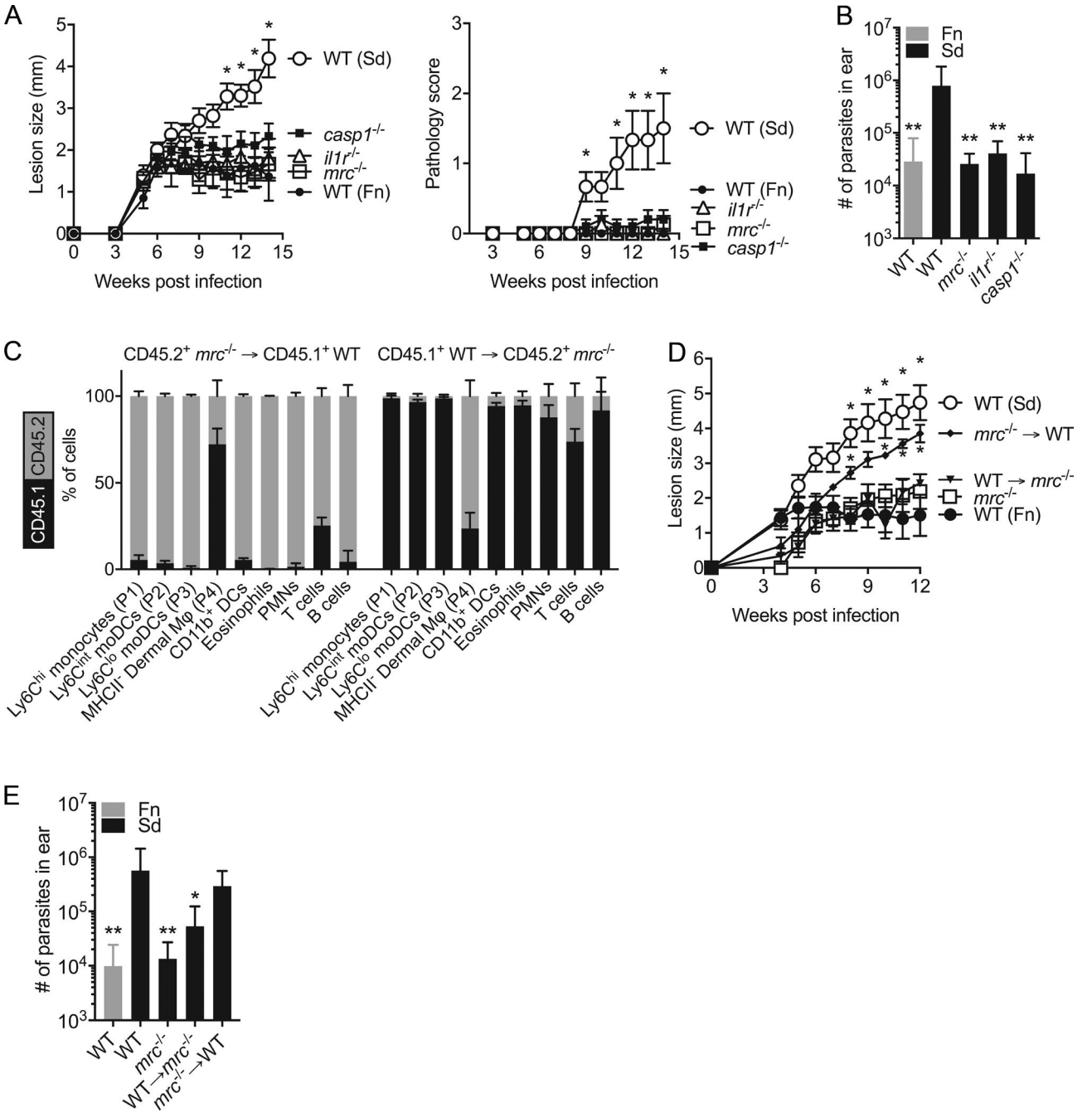

Figure 5. **Genetic ablation of MR on P4 dermal macrophages reverses nonhealing infection with LmSd. (A and B)** Lesion development and pathology scores (0 = no ulceration, 1 = ulcer, 2 = half ear eroded, 3 = ear completely eroded) over the course of infection (A) and parasite burdens at 15 wk p.i. with 10^3 LmSd metacyclic promastigotes in the ear dermis of indicated mice (B; n = 6–8; data representative of three independent experiments). **(C–E)** Reciprocal BM chimeras were generated between CD45.1$^+$ WT and CD45.2$^+$ *mrc*$^{-/-}$ mice. These BM chimeras were infected with 10^3 LmSd metacyclic promastigotes 4 wk after BM transfer. (C) The ratio between CD45.1$^+$ WT and CD45.2$^+$ *mrc*$^{-/-}$ cells from ear isolates of BM chimeras at 16 wk after BM transfer and 12 wk p.i. are shown (n = 10; data representative of two independent experiments). Each population was defined according to the gating scheme shown in Fig. S2 C using MR-independent markers. PMNs, polymorphonuclear leukocytes. (D and E) Lesion development (D) and parasite loads (E) at 12 wk p.i. are shown (n = 8–10; data representative of two independent experiments). Values represent mean ± standard deviation. *, $P < 0.05$; **, $P \leq 0.01$ by one-way ANOVA with Dunn's posttest compared with LmSd-infected WT (A, B, D, and E).

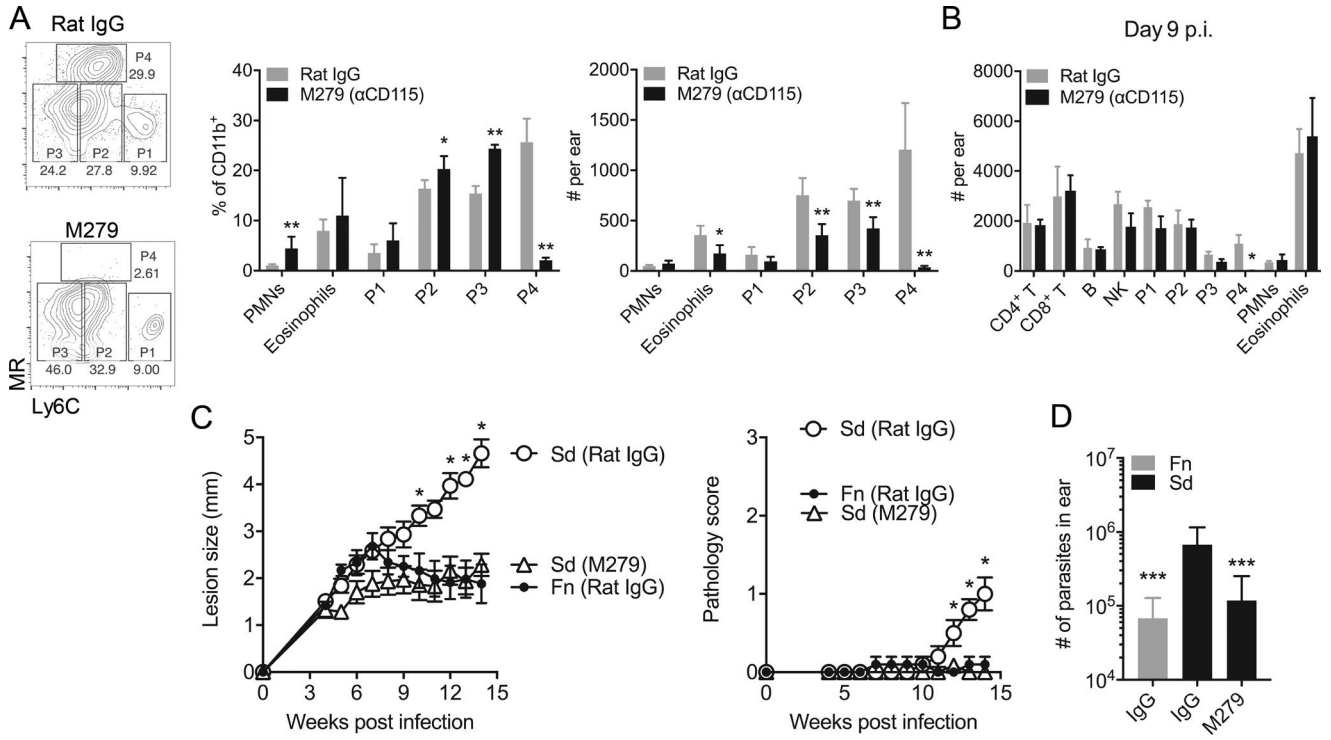

Figure 6. **Depletion of P4 dermal macrophages with anti–CSF-1R antibody ameliorates nonhealing infection with LmSd. (A)** Representative contour plots and bar graphs showing the frequency and total numbers of myeloid subsets recovered from the ear after treatment with M279 three times a week for 3 wk. **(B)** Total numbers of myeloid subsets recovered from the ears of control-treated or M279-treated mice for 3 wk and then infected for 9 d with 2 × 10^5 LmSd (n = 6; data representative of two independent experiments). PMNs, polymorphonuclear leukocytes. **(C and D)** Lesion development and pathology scores (0 = no ulceration, 1 = ulcer, 2 = half ear eroded, 3 = ear completely eroded) over the course of infection (C) and parasite burdens at 15 wk p.i. in the ear dermis of C57BL/6 mice treated with either M279 or control IgG three times a week for 9 wk (D; n = 8; data representative of two independent experiments). Mice were infected with 10^3 metacyclic promastigotes after the first 3 wk of treatment. Values represent mean ± standard deviation. *, P < 0.05; **, P ≤ 0.01; ***, P ≤ 0.0001 by nonparametric Mann-Whitney test (A and B) and by one-way ANOVA with Dunn's posttest compared with LmSd-infected WT (C and D).

P4 dermal macrophages maintain M2 functionality during infection

As previously described (Charmoy et al., 2016) and confirmed here using both tetramer staining and antigen restimulation of dermal and draining lymph node cells, *Leishmania*-specific T cell numbers and Th1 cytokine responses were found to be similar or higher in LmSd-infected compared with LmFn-infected mice (Fig. S4, A–C). Considering the strong production of IFN-γ and TNF-α in the LmSd-infected mice, we explored whether P4 dermal macrophages are able to maintain an M2 functionality during infection. Arginase 1 (Arg1) and RELM-α are well-described IL-4Rα–induced products that have proreparative functions (Allen and Sutherland, 2014). By intracellular staining of dermal cells from naive mice, we found no expression of iNOS or Arg1 in P1–P4 and only low expressions of Relm-α in P3 and P4 (Fig. 7 A). During the chronic stage of infection (9 and 12 wk p.i.), a high frequency of P1 and P2 and a lower frequency of P3, but virtually no P4, were $iNOS^+$. In contrast, a significant percentage of P4 recovered from the LmSd-infected mice were $Arg1^+$ and/or Relm-α^+. A similar fraction of P2 and P3 from these mice were also $Arg1^+$.

To elucidate the fate of the parasite inside the different populations recovered from infected ears, we sorted RFP^+ P1–P4 and assayed parasite survival and growth ex vivo (Fig. 7 B). Only the P4 dermal macrophages supported the growth of the parasite during the 48 h of ex vivo culture. Growth arrest or persistence of the parasite was observed over this time frame in P1–P3. Collectively, P4 dermal macrophages maintain their M2 phenotype even in a strong Th1 environment, and they remain permissive to intracellular growth of *L. major*.

IL-4 and IL-10 are essential to maintain the MR^{hi} P4 population during infection

Because IL-4 and/or IL-10 up-regulated MR on BMDM in vitro (Fig. 1 K), we were interested to know whether these cytokines might locally maintain MR expression on P4 in the face of the high levels of IFN-γ that would normally down-regulate MR (Schreiber et al., 1993). In IL-4– or IL-10–deficient naive mice, the numbers of MR^{hi} P4 cells were not altered (Fig. S5 A). In infected mice, however, the absence of IL-4 and/or IL-10 resulted in a significant de-

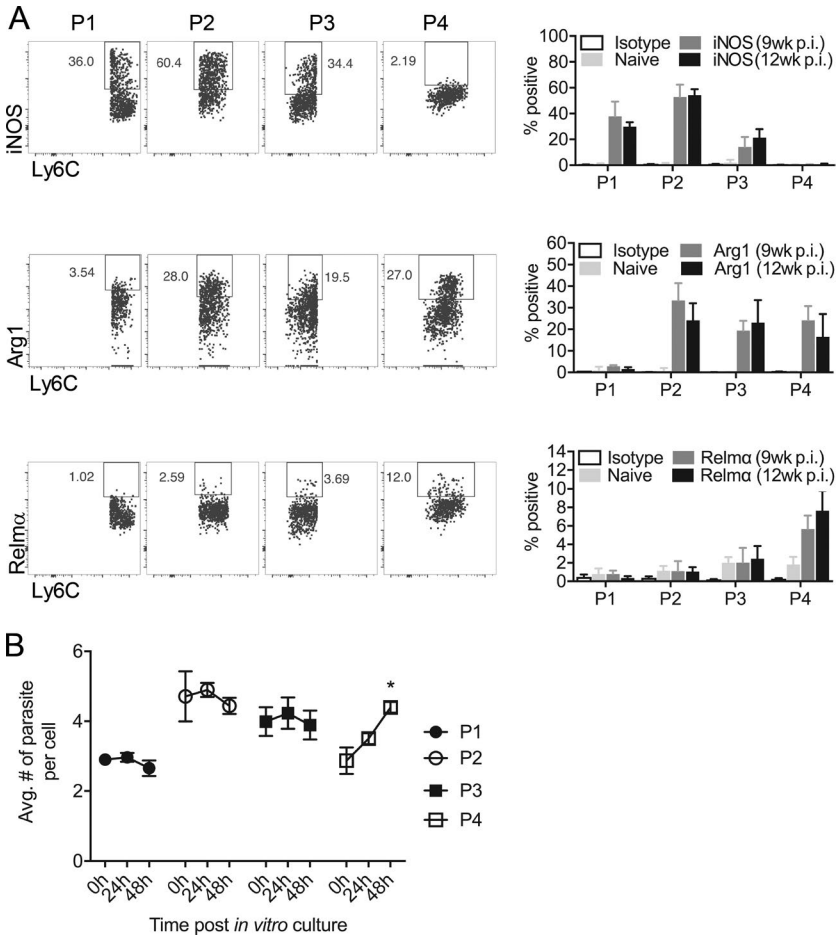

Figure 7. **P4 dermal macrophages express M2 functionality and remain permissive to LmSd infection. (A)** Representative dot plots and bar graphs showing the frequency of P1–P4 staining positive for iNOS, Arginase1, or Relm-α at 9 wk and 12 wk p.i. with 10^3 LmSd-RFP (n = 6; data representative of two independent experiments). **(B)** RFP$^+$ P1–P4 populations were sorted from C57BL/6 mice at 9 wk p.i. and incubated in vitro for 24–48 h. Giemsa-stained cells were scored for the mean number of parasites per infected cell at each time point (n = 4; data representative of two independent experiments). Values represent mean ± standard deviation. *, $P < 0.05$ by one-way ANOVA with Dunn's posttest compared with no incubation control (B).

crease in both the percentage and number of P4 relative to infected WT mice (Fig. 8 A). In contrast, the number of P1 and P2 was significantly increased, indicating the inhibitory effects of IL-4 and IL-10 on the recruitment or survival of monocytes and moDCs (Couper et al., 2008; Lazarski et al., 2013). Consistent with the lack of MR up-regulation on BMDM by IL-13 in vitro (Fig. 1 K), there was no change in the number or frequency of P1–P4 in IL-13$^{-/-}$–infected mice, whereas the recruitment of eosinophils was significantly decreased (Fig. S5 B).

We determined whether the deficit in the P4 population was caused only by the down-regulation of MR expression or also by the loss of these cells as defined using MR-independent markers (Fig. S2 C; Tamoutounour et al., 2013). Compared with WT mice, IL-4 and/or IL-10 deficiency resulted in a significant decrease both in the percentage of the CD11b$^+$ cells that were dermal macrophages and the level of MR expression on these cells (Fig. 8 B). Because IL-4 can induce local macrophage proliferation (Jenkins et al., 2011), we investigated whether there was IL-4–dependent expansion of P4 during LmSd infection (Fig. 8, C and D). On average, 5 and 1% of dermal macrophages in naive animals were Ki67 positive or BrdU incorporated, respectively, indicating a slow rate of self-renewal in steady state. At 12 d p.i., the P4 exhibited a two to threefold increase in the frequencies of Ki67$^+$ and BrdU$^+$ cells that were in each case abrogated in the IL-4–deficient mice, consistent with the small increase in the number of P4 cells during infection (Fig. 3 B). Notably, both IL-4Rα and IL-10Rα were expressed at higher levels on P4 than P1–P3 (Fig. 8 E). Collectively, during infection, IL-10 and to a lesser degree IL-4 are needed for MR expression, whereas IL-4 is needed to expand the population through local proliferation.

The LmSd infection outcomes were also monitored in the *il4*$^{-/-}$, *il10*$^{-/-}$, and *il4/10*$^{-/-}$ mice. As previously reported (Anderson et al., 2005), *il10*$^{-/-}$ mice had significantly lower parasite burdens than WT (Fig. 8 F). Interestingly, *il4/10*$^{-/-}$ mice had further decreased parasite counts compared with *il10*$^{-/-}$ mice. The role of IL-4 in promoting lesion development was apparent after 10 wk p.i., although the lesions still progressed in the *il4*$^{-/-}$ mice (Fig. 8 G). Despite the reduced parasite burdens, *il10*$^{-/-}$ and *il4/10*$^{-/-}$ mice showed comparable or exacerbated lesions compared with WT mice during the first 12 wk of infection, consistent with a critical role for IL-10 in modulating immune-mediated pathologies. However, lesions in all of the *il10*$^{-/-}$ and some of the *il4/10*$^{-/-}$ mice started to resolve or moderate after 12 wk p.i.

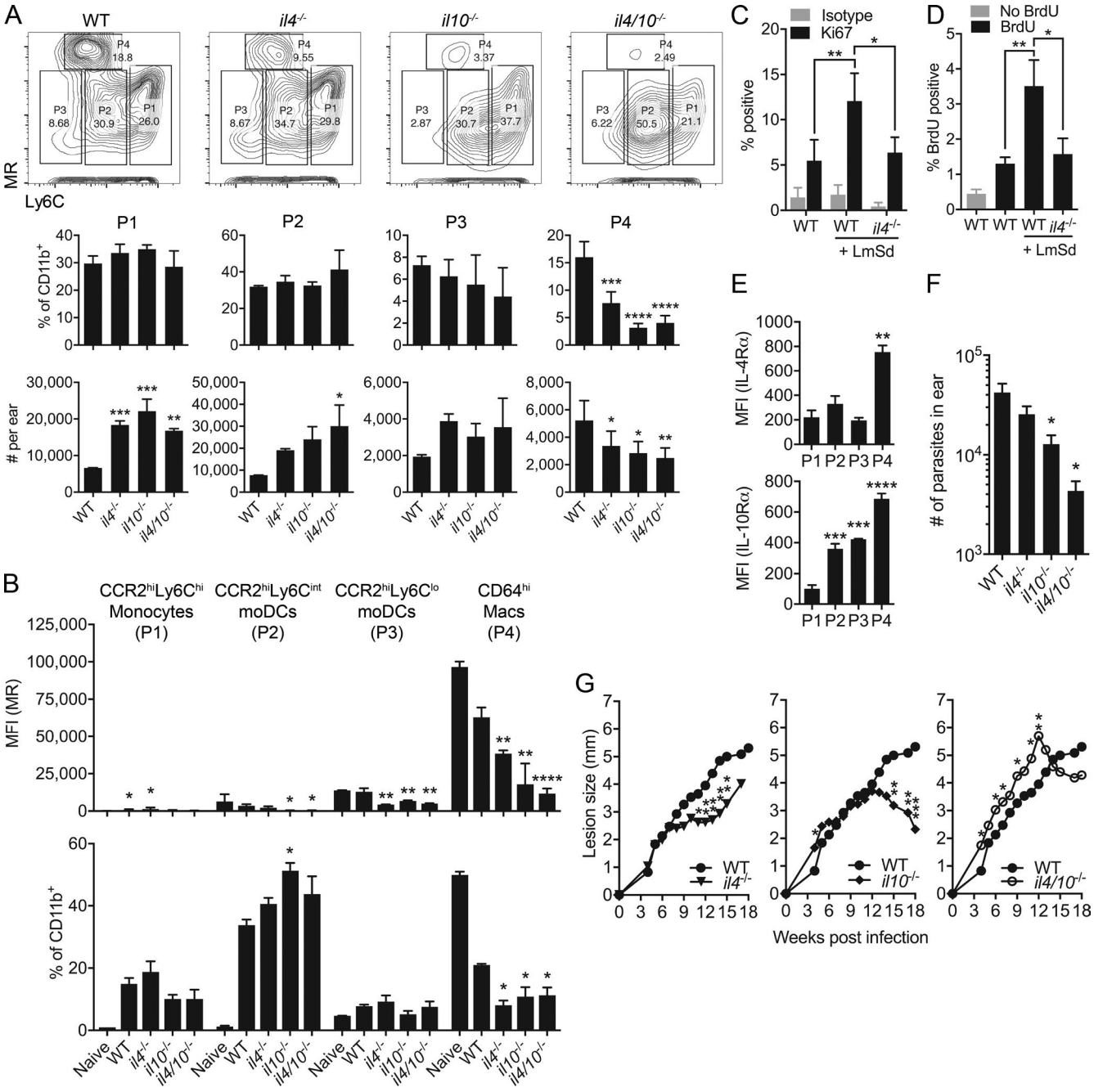

Figure 8. **P4 dermal macrophages are locally maintained by IL-4 and IL-10 during infection. (A)** Representative contour plots and bar graphs showing the frequency and absolute number of P1–P4 populations in C57BL/6, *il4*$^{-/-}$, *il10*$^{-/-}$, and *il4/10*$^{-/-}$ mice at day 12 p.i. with 2 × 10^5 LmSd. **(B)** The quantification of MR expression on CD11b$^+$CCR2^{hi}CD64^{lo}Ly6C^{hi}MHCII$^-$ monocytes, CD11b$^+$CCR2^{hi}CD64^{lo}Ly6C^{int}MHCII^{int} moDCs, CD11b$^+$CCR2^{hi}CD64^{lo}Ly6C^{lo}MHCII^{hi} moDCs, and CD11b$^+$CCR2^{lo}CD64^{hi}Ly6C^{int}MHCII$^-$ dermal macrophages in C57BL/6, *il4*$^{-/-}$, *il10*$^{-/-}$, and *il4/10*$^{-/-}$ mice at day 12 p.i. with 2 × 10^5 LmSd. The frequencies of the same populations were quantified in the bottom graph. **(C and D)** Ki67 expression or BrdU incorporation by P4 dermal macrophages from naive or infected WT and *il4*$^{-/-}$ mice at 12 d p.i. with 2 × 10^5 LmSd. (A–D) $n = 6$; data representative of two independent experiments. **(E)** Bar graphs showing the IL-4Rα and IL-10Rα expression levels on P1–P4 populations in naive C57BL/6 ($n = 4$; data representative of two independent experiments). Background MFIs of isotype controls were subtracted. **(F and G)** Parasite burdens at 2 wk p.i. with 2 × 10^5 metacyclic promastigotes (F; $n =$ 10; data representative of three independent experiments) and lesion development over the course of infection with 10^3 metacyclic promastigotes in the ear dermis of C57BL/6, *il4*$^{-/-}$, *Il10*$^{-/-}$, and *il4/10*$^{-/-}$ mice (G; $n = 8$–10; data representative of three independent experiments). Values represent mean ± standard deviation. *, $P < 0.05$; **, $P \leq 0.01$; ***, $P \leq 0.001$; ****, $P \leq 0.0001$ by nonparametric Mann-Whitney test (C, D, and G) and by one-way ANOVA with Dunn's posttest compared with WT C57BL/6 mice (A, B, and F) and P1 (E).

IL-1R and inflammasome activation contribute to P4 maintenance during infection

The IL-1β–inflammasome axis plays an essential role in the evolution of the nonhealing response (Charmoy et al., 2016). We were interested to understand how this innate response pathway might interplay with the disease-exacerbating mechanisms revealed in this study. We first determined that the source of IL-1β was not P4, but confined largely to P1–P3 (Fig. 9 A). We and others have previously reported that IL-1R signaling up-regulates IL-4 and IL-10 secretion and mRNA expression in *L. major*–infected mice (Kostka et al., 2006; Charmoy et al., 2016). In this study, the frequency of dermal $CD4^+$ T cells producing IL-4 and/or IL-10, already low in the WT mice, was significantly reduced in *casp1*$^{-/-}$ and *il1r*$^{-/-}$ mice, whereas the frequency of IFN-γ^+ T cells was increased (Fig. 9 B). Accordingly, the number of P4 dermal macrophages was significantly reduced in the LmSd-infected *casp1*$^{-/-}$ and *il1r*$^{-/-}$ mice (Fig. 9 C). The number of eosinophils was also reduced.

DISCUSSION

In this study, we explore the infection and activation states of myeloid subsets in the dermis of conventionally resistant C57BL/6 mice infected with a healing and nonhealing strain of *L. major*. We identify a population of MR^{hi} dermal macrophages that is present in the steady-state dermis and is preferentially infected by LmSd in an MR-dependent manner to promote nonhealing cutaneous disease. The MR^{hi} dermal macrophages are radio resistant and only minimally replaced by monocytes or adult BM–derived precursors during infection. Their self-renewal is M-CSF dependent in the steady state and requires IL-4 during infection. They maintain M2-associated markers and remain permissive to *L. major* growth despite the high levels of IFN-γ and TNF-α that activate monocyte-derived subsets for controlling parasites within the same tissue environment.

The MR^{hi} population described here provides clear evidence that there is a substantial M2-like population present in the steady-state dermis. The population was identified by combining MR and Ly6C staining on $CD11b^+lin^-$ cells and comparing them with the markers previously used to define dermal macrophages ($CD64^{hi}Ly6C^{int}CCR2^{lo}MHCII^{+/-}$; Tamoutounour et al., 2013). MR up-regulation on macrophages in response to type 2 cytokines provided one of the first markers for their alternative activation state (Stein et al., 1992; Martinez-Pomares et al., 2003). MR functions as a scavenger of blood-circulatory glycoproteins that are elevated in inflammation and wound healing (Lee et al., 2002). We showed that MR^{hi} dermal macrophages rapidly scavenged high–molecular weight dextran from blood lumen, which was reported to be MR dependent and a characteristic of skin trans-endothelial, radio-resistant macrophages, termed STREAMs (Wollenberg et al., 2002; Barreiro et al., 2016). We also showed that the dermal macrophages efficiently captured apoptotic cells and up-regulated an additional set of M2-associated molecules, including PtdSer receptors, scavenger receptors, angiogenic factors, and C-type lectins. A related panel of molecules was found to be transcriptionally up-regulated in the dermal macrophages previously described (Tamoutounour et al., 2013). Altogether, these molecular and functional attributes suggest that the MR^{hi} dermal macrophages have important homeostatic functions related to tissue repair and the resolution of inflammation. It is important to emphasize that the designation of the P4 population as M2-like encompasses macrophages with broadly antiinflammatory, reparative phenotypes and that their gene expression profiles are likely to be distinct from other designated M2 populations that have been conditioned by a unique set of mediators and microbial stimuli in vivo or in vitro (Murray et al., 2014).

Most peripheral tissues are populated early during embryogenesis by yolk sac– or fetal liver–derived macrophages that are self-renewed in situ (Ginhoux et al., 2010; Yona et al., 2013). Dermal macrophages are thought to be an exception to this ontogenic scheme because in the two studies addressing this question, a substantial fraction of these cells originated from the parabiotic partner (Jakubzick et al., 2013; Tamoutounour et al., 2013), implicating a contribution from blood precursors. In contrast, our data pertaining to the P4 population and using multiple approaches to study its renewal by monocyte-derived or adult BM–derived precursors indicate minimal replacement by these cells, even during the first weeks of infection when there were high numbers of monocytes recruited to the site. The inconsistencies in the extent of donor exchange in the parabiotic partners, comparing the prior studies with our own, likely reflect the steady-state versus infection conditions analyzed. Our study highlights the self-turnover of dermis macrophages that is IL-4 dependent during *L. major* infection. In this regard, the findings share some similarities with the first study to describe localized macrophage renewal, in which helminth infection in the pleural cavity resulted in IL-4–dependent proliferative expansion of resident macrophages with minimal recruitment of adult BM–derived cells (Jenkins et al., 2011). A key distinction of our study, however, is that the self-renewal of dermal macrophages and their maintenance as M2-like cells occurred not within the context of a helminth-driven, polarized type 2 response, but within the strong proinflammatory environment of the *L. major*–loaded dermis.

In this study, *L. major* infection induced an $iNOS^{neg}$ $Arg1^{hi}Relm\text{-}\alpha^{pos}$ response in at least a fraction of the P4 population even as the Th1 response strongly up-regulated iNOS expression in the inflammatory monocytes and moDCs. Our results suggest that so long as the P4 population remained locally conditioned by IL-4 and IL-10 during infection, its size and M2 functionality such as MR expression were maintained. The up-regulated expression of IL-4Rα and IL-10Rα on the P4 population likely explains how these cells remain responsive to the relatively low levels of IL-4 and IL-10 produced in the site. In addition, there may be a close tissue association between the

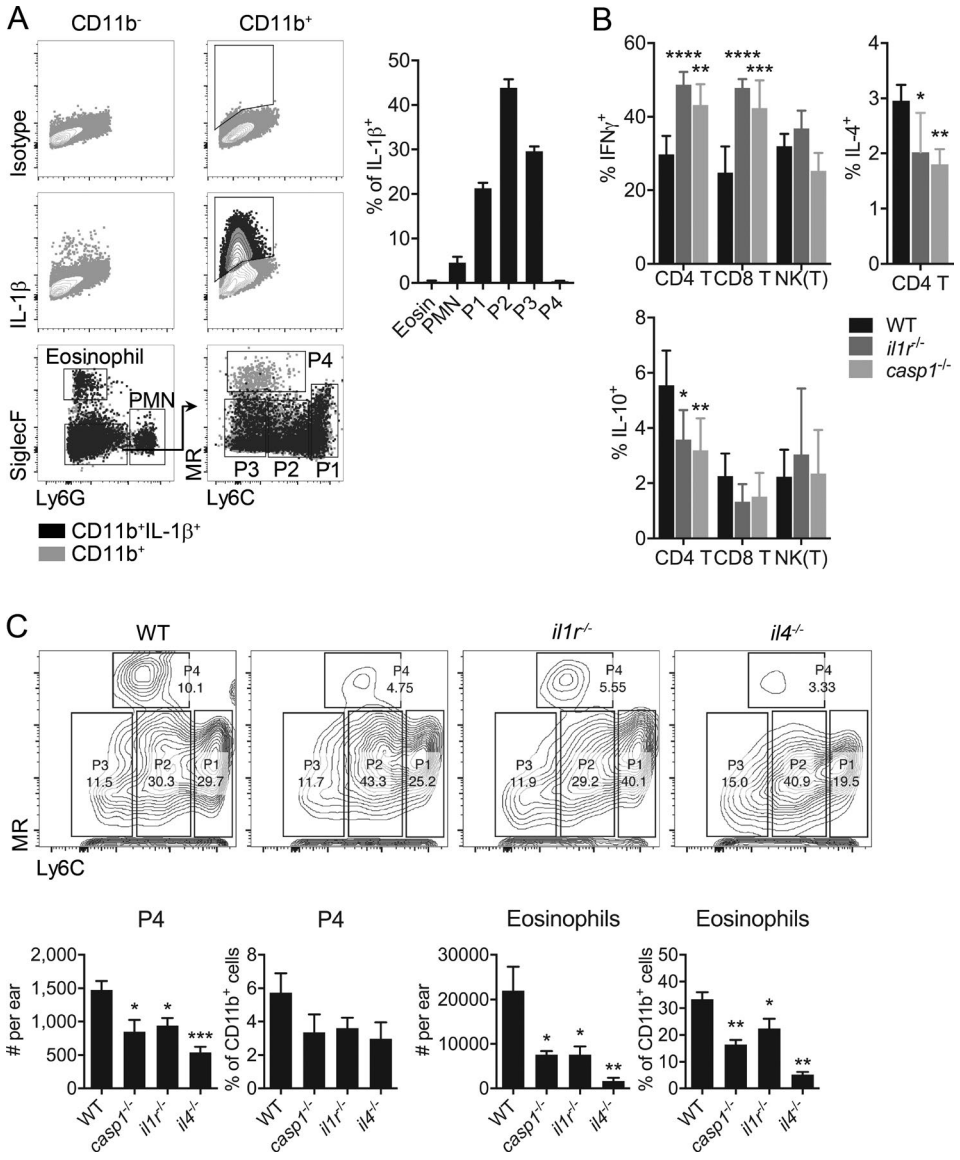

Figure 9. **IL-1R and inflammasome activation contribute to the maintenance of the P4 dermal macrophages during infection. (A)** Representative dot plots and bar graph showing the frequency of CD11b$^+$IL-1β$^+$ cells overlaid onto CD11b$^+$ cells from C57BL/6 mice infected with 10^3 LmSd and recovered from the ear dermis at 12 wk p.i. (n = 4; data representative of three independent experiments). **(B)** The frequency of CD4$^+$ T, CD8$^+$ T, and natural killer T cells (NK[T]) in ear lesions stained positive for IFN-γ, IL-10, and IL-4 at 12 wk p.i. with 10^3 LmSd (n = 6; data representative of three independent experiments). **(C)** Representative dot plots show the frequency of dermal P1–P4 populations in C57BL/6, *casp1*$^{-/-}$, *il1r*$^{-/-}$, and *il4*$^{-/-}$ mice at 12 wk p.i. with 10^3 LmSd. Bar graphs show the absolute number and frequency of P4 and eosinophils (n = 6–8; data representative of three independent experiments). Values represent mean ± standard deviation. *, P < 0.05; **, P ≤ 0.01; ***, P ≤ 0.001; ****, P ≤ 0.0001 by one-way ANOVA with Dunn's posttest compared with WT C57BL/6 mice (B and C).

cells that produce these cytokines and the dermal macrophages that favors their compartmentalized response. A recent study showed that genetic deletion of TNF strongly up-regulated Arg1 and down-regulated iNOS in monocyte-derived inflammatory cells despite a prominent Th1 response during *L. major* infection, suggesting that the P4 dermal macrophages may have lost their responsiveness to TNF that would normally function to antagonize their alternative activation (Schleicher et al., 2016). Their functional specialization for apoptotic cell capture (Fig. 2 F) might also contribute to the signals that establish and maintain their M2 activation program. It was reported that coordinated signals involving type 2 cytokines and recognition of apoptotic cells were required to maintain the reparative function of tissue-resident macrophages during inflammation in the lung and the gut (Bosurgi et al., 2017).

In contrast to P4 dermal macrophages, TNF-α– and iNOS-producing dermal DCs of monocyte origin have been previously associated with the control of *L. major* infection (Wei et al., 1995; Stenger et al., 1996; De Trez et al., 2009). Our own findings in P1–P3 confirm the coexpression of iNOS and Arg1 in monocyte-derived cells from *L. major*–infected C57BL/6 mice reported previously (Schleicher et al., 2016) and are consistent with prior studies showing Arg1 production by M1-polarized cells in other infection models (El Kasmi et al., 2008; Qualls et al., 2010). The phenotype of P1–P3 populations may explain why these cells continue to be parasitized during the chronic phase of *L. major* infection and may contribute to the lack of parasite control in LmSd-infected mice.

The size of the P4 population was significantly decreased by the absence of IL-1R or caspase-1/11, consistent with the requirement for inflammasome-dependent IL-1β for the evolution of the nonhealing phenotype (Charmoy et al., 2016). We and others previously observed (Charmoy et al., 2016) and confirm here that the production of IL-4 and IL-10 is decreased and the production of IFN-γ is increased during infection in the absence of IL-1R or caspase 1/11. There is accumulating evidence that IL-1R signaling can promote Th2 development (Santarlasci et al., 2013). Of particular relevance to the current study, the conversion of monocyte-derived macrophages to an alternatively activated state with reparative function in the liver after infection with *Listeria monocytogenes* relied on an IL-1β–caspase-1–dependent pathway of IL-4 secretion by basophils (Blériot et al., 2015). We are currently investigating multiple possible cellular sources of IL-4, including eosinophils that infiltrate *Leishmania*-infected skin and can be potent producers of IL-4 (Rothenberg and Hogan, 2006).

Our data confirm that CSF-1 is a survival factor for dermal macrophages under steady-state conditions. Although the monocyte-derived populations were also partially depleted in the naive skin by the CSF-1R blockade, only the dermal macrophages remained significantly depleted in the infected skin. This is in agreement with the lack of effect of CSF-1R blockade on monocyte recruitment in other inflammatory models, including wound healing (MacDonald et al., 2010). The requirement of prolonged treatment of M279 for a complete depletion of P4 is consistent with a prior study (Sauter et al., 2014) and concurs with their slow rate of turnover, as shown in the Ki67 staining and BrdU incorporation. CSF-1R blockade is currently being used as a strategy to inhibit the tumor-promoting function of tumor-associated macrophages that is thought to rely on their M2 activated state (Pyonteck et al., 2013).

MR recognizes the mannose-containing moieties of a variety of microorganisms (Linehan et al., 2000). We showed that treatment of BMDMs with BSA-mannose significantly decreased LmSd infection, but not LmFn infection in vitro, and that stronger M2 polarization using IL-4 and IL-10 further up-regulated MR and augmented the favored uptake of LmSd versus LmFn. Differences in the oligosaccharide structures of the major surface lipophosphoglycans of LmSd and LmFn promastigotes have been described that might account for the differences in MR-mediated uptake (Sacks and da Silva, 1987). However, because the selective recognition extended to the amastigote stage that is largely devoid of lipophosphoglycan, the involvement of other mannose-containing glycoconjugates is indicated. Our finding that the in vitro behavior of LmSd×LmFn hybrids generated by sexual crosses precisely predicted their healing or nonhealing phenotypes in vivo reinforces the link between the differential targeting of MR^{hi} macrophages and clinical outcome and offers the possibility to use a forward genetic approach to identify the parasite ligands involved.

MR-mediated infection of tissue-resident macrophages that maintain an M2 activation program is a possible immune evasive strategy used by other intracellular pathogens. For example, MR plays an important role in the phagocytosis of a virulent but not an attenuated strain of *Mycobacterium tuberculosis* (Schlesinger, 1993). Reagents that specifically target the CD206 macrophage MR in humans are being developed for diagnostic imaging and therapy to inhibit tumor progression (Cope et al., 2016). The clinical relevance of our findings can be inferred from the fact that the LmSd strain was isolated from a patient with chronic lesions and persisting organisms even after treatment and despite a strong cell-mediated immune response to *Leishmania* antigens (Neva et al., 1979). Our study provides a rationale for therapeutic targeting of MR^{hi} dermis-resident macrophages for the treatment of chronic forms of cutaneous leishmaniasis.

MATERIALS AND METHODS

Mice

C57BL/6 mice were purchased from Taconic Farms. C57BL/6 *IL1r1*$^{-/-}$, C57BL/6 *Casp1/11*$^{-/-}$, C57BL/6 *il4*$^{-/-}$, C57BL/10 *il10*$^{-/-}$, C57BL/6 *il13*$^{-/-}$, C57BL/6 *il4*$^{-/-}$*il10*$^{-/-}$, CD45.1^{+} B6.SJL, and CD45.1^{+}*cx3cr1*$^{gfp/+}$ (B6.SJL-Cd45a (Ly5a)/Nai×C57BL/6-CD45a-[KO]CX3CR1-[KI]EGFP F1) mice were obtained through a supply contract between the National Institute of Allergy and Infectious Diseases (NIAID) and Taconic Farms. C57BL/6J *cr3*$^{-/-}$ (*itgam*^{tm1Myd}), C57BL/6J *c3*$^{-/-}$ (*c3*^{tm1Crr}), and C57BL/6J *il10*^{gfp} (*il10*$^{Tm1.1Karp}$) mice were purchased from The Jackson Laboratory. C. Bosio (NIAID, National Institutes of Health, Bethesda, MA) provided C57BL/6 *mrc*$^{-/-}$ mice. All the mice used in these experiments were females and were maintained in the NIAID animal care facility under specific pathogen-free conditions, used under a study protocol approved by the NIAID Animal Care and Use Committee (protocol no. LPD 68E). All aspects of the use of animals in this research were monitored for compliance with the Animal Welfare Act, the Public Health Service Policy, the U.S. Government Principles for the Utilization and Care of Vertebrate Animals Used in Testing, Research, and Training, and the National Institutes of Health Guide for the Care and Use of Laboratory Animals.

In vivo injections

M279 (Amgen) is a rat IgG mAb, which blocks ligand binding to the CSF-1R. In this study, mice were treated with 200 µg M279 or rat IgG (Sigma-Aldrich) intraperitoneally three times a week for 9 wk. Manocept–Alexa Fluor 488 (Navidea Biopharmaceuticals) is a fluorescently labeled derivative of FDA-approved 99MTC-Tilmanocept targeting MR. Naive mice were injected with Manocept–Alexa Fluor 488 intradermally and intravenously and sacrificed 1 and 2 h later, respectively, for analysis. Naive mice were also injected intravenously with 1% (wt/vol) of 2-MD FITC-dextran (Sigma-Aldrich) or 10 µg of anti–mouse CD206 (C068C2; Biolegend) and sacrificed 10–30 and 3 min later, respectively. For measuring apoptotic cell uptake, 10^6 thymocytes were treated for 6 h with 1 µM dexamethasone (Sigma-Aldrich) and were intradermally injected into naive mice.

L. major infection and lesion measurements

LmSd (MHOM/SN/74/SD) and LmFn (MHOM/IL/80/Friedlin) were maintained as follows: promastigotes were grown at 26°C in medium 199 (M199) supplemented with 20% heat-inactivated FCS (Gemini Bio-Products), 100 U/ml penicillin, 100 µg/ml streptomycin, 2 mM L-glutamine, 40 mM Hepes, 0.1 mM adenine (in 50 mM Hepes), 5 mg/ml hemin (in 50% triethanolamine), and 1 mg/ml 6-biotin (M199/S). Parasites expressing an RFP (LmFn-RFP and LmSd-RFP) were grown using the identical culture medium supplemented with 50 µg/ml Geneticin (G418; GIBCO BRL). Infective-stage metacyclic promastigotes were isolated from stationary cultures (5–6 d) by density gradient centrifugation as described previously (Späth and Beverley, 2001). Mice were then inoculated with 1,000 or 200,000 metacyclic promastigotes in the ear dermis by intradermal injection in a volume of 10 µl. Lesion development was monitored weekly by measuring the diameter of the ear nodule with a direct-reading Vernier caliper (Thomas Scientific).

Processing of ear tissues and evaluation of parasite burden

Ear tissue was prepared as previously described (Belkaid et al., 2000). In brief, the two sheets of infected ear dermis were separated, deposited in DMEM containing 0.2 mg/ml Liberase TL–purified enzyme blend (Roche Diagnostics Corp.), and incubated for 1.5 h at 37°C. Digested tissue was processed in a tissue homogenizer for 3.5 min (Medimachine; Becton Dickinson) and filtered through a 70-µm cell strainer (Falcon Products). Parasite titrations were performed as previously described (Belkaid et al., 1998). In brief, tissue homogenates were serially diluted in 96-well, flat-bottom microtiter plates containing 100 µl M199/S. The number of viable parasites in each ear was determined from the highest dilution at which promastigotes could be grown out after 7–10 d of incubation at 26°C.

Immunolabeling and flow cytometry analysis

Single-cell suspensions were stained with a LIVE/DEAD Fixable Aqua Dead Cell Stain kit (Thermo Fisher) and incubated with an anti–Fc-γ II/III (CD16/32) receptor antibody (2.4G2; BD Biosciences) in PBS containing 1% FCS followed by fluorochrome-conjugated antibodies for 1 h on ice. The following antibodies were used for surface staining: FITC, APC/Cy7, and Brilliant Violet 421 anti–mouse Ly6G (1A8; Biolegend); APC/Cy7 anti–mouse Ly6C (HK1.4; Biolegend); PE/Cy7 anti–mouse CD11b (M1/70; Biolegend); FITC anti–mouse CD4 (GK1.5; Biolegend); PerCP/Cy5.5 and APC anti–mouse CD8-α (53-6.7; Biolegend); PerCP/Cy5.5, Brilliant Violet 421, and APC/Cy7 anti–mouse NK1.1 (PK136; Biolegend); Alexa Fluor 647 and APC anti–mouse CD206 (C068C2; Biolegend); PE and Brilliant Violet 421 anti–mouse Siglec-F (E50-2440; BD Biosciences); FITC and PE anti–mouse CD45.1 (A20; Biolegend); PerCP/Cy5.5 anti–mouse CD45.2 (104; Biolegend); PE anti–mouse IL-10Rα (1B1.3a; Biolegend); PE anti–mouse IL-4Rα (I015F8, Biolegend); PE anti–mouse CD36 (HM36; Biolegend); PE anti–mouse CD301 (LOM-14; Biolegend); PE anti–mouse DC-SIGN (902404; R&D Systems); PE anti–mouse TGFR2 (R&D Systems); biotin anti–mouse COLEC12 (R&D Systems) with PE-streptavidin (Biolegend); FITC anti–mouse MHCII (AF6-120.1; Biolegend); PE anti–mouse CCR2 (475301; R&D Systems); PerCP/Cy5.5 anti–mouse CD64 (X54-5/7.1; Biolegend); PerCP/Cy5.5 anti–mouse TCR-β (H57-597; Biolegend); PerCP/Cy5.5 anti–mouse B220 (RA3-6B2; Biolegend); PE anti–mouse Lyve-1 (223322; R&D Systems); PE anti–mouse MERTK (2B10C42; Biolegend); and PE anti–mouse Tim-4 (RMT4-54; Biolegend). For intracellular detection of cytokines, cells were cultured in the presence of 20 ng/ml PMA and 700 ng/ml ionomycin in the presence of GolgiStop protein transport inhibitor (BD Biosciences) for 4 h at 37°C. The staining of surface and cytoplasmic markers was performed sequentially. Cells were first incubated with a LIVE/DEAD Fixable Aqua Dead Cell Stain kit. They were stained for their surface markers, then fixed and permeabilized using Cytofix/Cytoperm (BD Biosciences), and finally stained for detection of intracellular molecules for 30 min on ice. The following antibodies were used for cytokine detection: PE anti–mouse IL-1β proform (NJTEN3; eBioscience); APC anti–mouse IL-2 (JES6-5H4; eBioscience); PE and PE/Cy7 anti–mouse IFN-γ (XMG1.2; eBioscience); PE anti–mouse IL-4 (11B11; eBioscience); PE and Brilliant Violet 421 anti–mouse IL-10 (JES5-16E3; eBioscience); PE anti-mouse TNF-α (TN3-19; eBioscience); APC anti–mouse Arginase1 (R&D Systems); Alexa Fluor 488 anti–mouse iNOS (CXNFT; eBioscience); and biotinylated anti–mouse Relm-α (Peprotech). For detection of antigen-specific $CD4^+$ T cells, single-cell suspensions were stained with PE glycosomal phosphoenolpyruvate carboxykinase–tetramer ($I\text{-}A^b$ *L. major* GPC 335-351 NDAFGV MPPVARLTPEQ) and PE and APC Clip-tetramer ($I\text{-}A^b$ human CLIP 87-101 PVSKMRMATPLLMQA) for 1 h at room temperature before surface staining. The data were collected using FacsDIVA software and a flow cytometer (FacsCANTO II; BD Biosciences) and analyzed with FlowJo

software (Tree Star). To measure in vivo cell proliferation, mice were intravenously injected with 2 mg BrdU (eBioscience) in PBS. After 3 h, intracellular staining for Ki67 and incorporated BrdU were performed using eBioscience kits according to the manufacturer's instructions.

BMDM generation, infection, and in vitro treatment

Isolated femurs and tibia were flushed with PBS, and precursor cells were cultured in complete RPMI supplemented with 30% L929 cell–conditioned medium. After 7 d in culture, mature BMDMs were further incubated with M1- or M2-inducing stimuli (10 ng/ml IFN-γ, 50 ng/ml LPS, 20 ng/ml IL-4, 10 ng/ml IL-10, or 10 ng/ml IL-13; Peprotech) or harvested by washing with cold PBS, incubating on ice for 15 min, and pipetting extensively. 5×10^4 BMDMs/well were plated onto an 8-well Permanox chamber slide (Thermo Fisher) in complete RPMI and infected with metacyclic promastigotes and amastigotes at different multiplicities of infection (MOIs) with or without BSA-mannose (Vector Laboratories) and RGDS (Sigma-Aldrich) pretreatment. After infection, BMDMs were washed three times with PBS to remove free parasites and further incubated in complete RPMI for Wright-Giemsa staining (Thermo Fisher). To acquire amastigotes, infected BMDMs were lysed by passing through 25-gauge needles in amastigote media (50 mM glucose and 20 mM EDTA in PBS) and spun at 300 *g* for 10 min. Supernatant cells were pelleted and washed two times with amastigote media at 3,000 *g* for 15 min.

BM chimera generation

Recipient mice were irradiated with a single dose of 1,250 rads and reconstituted with donor BM. The harvested BM cells were injected intravenously at a dose of 2.5×10^6 cells/mouse in 100 µl PBS. Animals were maintained on trimethoprim-sulfamethoxazole (Hi-Tech Pharmacal) antibiotic water for up to 5 wk after irradiation. Hematopoietic reconstitution of all animals was verified by FACS staining of splenocytes and ear isolates.

Adoptive transfer of monocytes

For adoptive transfer, total monocytes from the BM of CD45.1$^+$ *cx3cr1*$^{gfp/+}$ mice were sorted on a monocyte isolation kit (Miltenyi Biotec) as EGFP$^+$ to a purity of >95%. For homing experiments, cells were injected intravenously (2×10^6 cells) into C57BL/6 recipient mice at 7 d p.i. with 2×10^5 LmSd. Ear tissues were processed, and the homing of GFP$^+$ monocytes was analyzed by flow cytometry at 1, 3, and 5 d after the injection.

Parabiosis

7–8-wk-old female CD45.2$^+$ C57BL/6 and CD45.1$^+$ B6.SJL mice were matched for body weight and cohoused for 2 wk. Pairs were surgically connected as previously described (Wright et al., 2001).

Confocal microscopy

LmSd-RFP–infected mouse ears were mounted in Tissue-Tec OCT (Sakura Finetek). 12-µm cryostat-cut sections were placed onto Superfrost Plus microscope slides (Thermo Fisher) and allowed to dry for 5 min. Before immunostaining, the slides were rehydrated in PBS for 5 min. For immunohistochemistry, the sections were blocked with 10% FCS in PBS and incubated with APC anti–mouse CD206 (C068C2; Biolegend). After 1 h of incubation (at 37°C temperature in a humidified chamber), the slides were washed in PBS for 10 min and stained with Hoechst 33342 (Thermo Fisher). The samples were analyzed with a confocal laser fluorescence microscope (SP8; Leica) and Imaris software (Bitplane).

Statistical analyses

The differences in values obtained for two different groups were determined using a nonparametric Mann-Whitney test. For comparisons of multiple groups, ANOVA followed by Dunn's posttest was used. Analyses were performed using Prism 6.0f software (GraphPad).

Online supplemental material

Fig. S1 shows the healing and nonhealing cutaneous infection of C57BL/6 mice by LmFn and LmSd, respectively, in terms of lesion size and pathology score. Fig. S2 shows selective uptake of Manocept–Alexa Fluor 488 by P4 dermal macrophages, the comparison of P1–P4 populations with previously reported dermal myeloid populations (Tamoutounour et al., 2013), and histograms of M2 markers expressed on P1–P4 in a naive state. Fig. S3 analyzes effects of an extended blockade of CSF-1R signaling by anti-CSFR antibody (M279). Fig. S4 shows that LmFn and LmSd had no significant difference in both antigen-specific T cell development and cytokine production from T cells. Fig. S5 shows no difference in the number or the percentage of P4 in naive WT, IL-4$^{-/-}$, IL-10$^{-/-}$, and IL-4/10$^{-/-}$ mice or in infected IL-13$^{-/-}$ mice.

ACKNOWLEDGMENTS

We thank Dr. Catherine Bosio for the *mrc*$^{-/-}$ mice; Dr. Owen Schwartz (NIAID) and Dr. Sundar Ganesan (NIAID) for help with image acquisition and analysis; and Dr. Calvin Eigsti (NIAID) for help with the cell sorting.

This work was supported in part by the Intramural Research Program of the NIAID, National Institutes of Health.

The authors declare no competing financial interests.

Author contributions: S.H. Lee and D.L. Sacks designed the study. S.H. Lee, M. Charmoy, A. Romano, A. Paun, M.M. Chaves, F.O. Cope, and D.A. Ralph performed experiments. S.H. Lee and D.L. Sacks analyzed the data and wrote the manuscript.

Submitted: 3 August 2017

Revised: 21 September 2017

Accepted: 10 November 2017

REFERENCES

Akilov, O.E., R.E. Kasuboski, C.R. Carter, and M.A. McDowell. 2007. The role of mannose receptor during experimental leishmaniasis. *J. Leukoc. Biol.* 81:1188–1196. https://doi.org/10.1189/jlb.0706439

Allen, J.E., and T.E. Sutherland. 2014. Host protective roles of type 2 immunity: parasite killing and tissue repair, flip sides of the same coin. *Semin. Immunol.* 26:329–340. https://doi.org/10.1016/j.smim.2014.06.003

Anderson, C.F., S. Mendez, and D.L. Sacks. 2005. Nonhealing infection despite Th1 polarization produced by a strain of Leishmania major in C57BL/6 mice. *J. Immunol.* 174:2934–2941. https://doi.org/10.4049/jimmunol.174.5.2934

Azad, A.K., M.V. Rajaram, W.L. Metz, F.O. Cope, M.S. Blue, D.R. Vera, and L.S. Schlesinger. 2015. γ-Tilmanocept, a New Radiopharmaceutical Tracer for Cancer Sentinel Lymph Nodes, Binds to the Mannose Receptor (CD206). *J. Immunol.* 195:2019–2029. https://doi.org/10.4049/jimmunol.1402005

Barreiro, O., D. Cibrian, C. Clemente, D. Alvarez, V. Moreno, Í. Valiente, A. Bernad, D. Vestweber, A.G. Arroyo, P. Martín, et al. 2016. Pivotal role for skin transendothelial radio-resistant anti-inflammatory macrophages in tissue repair. *eLife.* 5:5. https://doi.org/10.7554/eLife.15251

Belkaid, Y., S. Kamhawi, G. Modi, J. Valenzuela, N. Noben-Trauth, E. Rowton, J. Ribeiro, and D.L. Sacks. 1998. Development of a natural model of cutaneous leishmaniasis: powerful effects of vector saliva and saliva preexposure on the long-term outcome of *Leishmania major* infection in the mouse ear dermis. *J. Exp. Med.* 188:1941–1953. https://doi.org/10.1084/jem.188.10.1941

Belkaid, Y., S. Mendez, R. Lira, N. Kadambi, G. Milon, and D. Sacks. 2000. A natural model of Leishmania major infection reveals a prolonged "silent" phase of parasite amplification in the skin before the onset of lesion formation and immunity. *J. Immunol.* 165:969–977. https://doi.org/10.4049/jimmunol.165.2.969

Blériot, C., T. Dupuis, G. Jouvion, G. Eberl, O. Disson, and M. Lecuit. 2015. Liver-resident macrophage necroptosis orchestrates type 1 microbicidal inflammation and type-2-mediated tissue repair during bacterial infection. *Immunity.* 42:145–158. https://doi.org/10.1016/j.immuni.2014.12.020

Bosurgi, L., Y.G. Cao, M. Cabeza-Cabrerizo, A. Tucci, L.D. Hughes, Y. Kong, J.S. Weinstein, P. Licona-Limon, E.T. Schmid, F. Pelorosso, et al. 2017. Macrophage function in tissue repair and remodeling requires IL-4 or IL-13 with apoptotic cells. *Science.* 356:1072–1076. https://doi.org/10.1126/science.aai8132

Charmoy, M., B.P. Hurrell, A. Romano, S.H. Lee, F. Ribeiro-Gomes, N. Riteau, K. Mayer-Barber, F. Tacchini-Cottier, and D.L. Sacks. 2016. The Nlrp3 inflammasome, IL-1beta, and neutrophil recruitment are required for susceptibility to a non-healing strain of Leishmania major in C57BL/6 mice. *Eur. J. Immunol.* 46:897–911.

Cope, F.O., B. Abbruzzese, J. Sanders, W. Metz, K. Sturms, D. Ralph, M. Blue, J. Zhang, P. Bracci, W. Bshara, et al. 2016. The inextricable axis of targeted diagnostic imaging and therapy: An immunological natural history approach. *Nucl. Med. Biol.* 43:215–225. https://doi.org/10.1016/j.nucmedbio.2015.11.007

Couper, K.N., D.G. Blount, and E.M. Riley. 2008. IL-10: the master regulator of immunity to infection. *J. Immunol.* 180:5771–5777. https://doi.org/10.4049/jimmunol.180.9.5771

De Trez, C., S. Magez, S. Akira, B. Ryffel, Y. Carlier, and E. Muraille. 2009. iNOS-producing inflammatory dendritic cells constitute the major infected cell type during the chronic Leishmania major infection phase of C57BL/6 resistant mice. *PLoS Pathog.* 5:e1000494. https://doi.org/10.1371/journal.ppat.1000494

El Kasmi, K.C., J.E. Qualls, J.T. Pesce, A.M. Smith, R.W. Thompson, M. Henao-Tamayo, R.J. Basaraba, T. König, U. Schleicher, M.S. Koo, et al. 2008. Toll-like receptor-induced arginase 1 in macrophages thwarts effective immunity against intracellular pathogens. *Nat. Immunol.* 9:1399–1406. https://doi.org/10.1038/ni.1671

Gautier, E.L., T. Shay, J. Miller, M. Greter, C. Jakubzick, S. Ivanov, J. Helft, A. Chow, K.G. Elpek, S. Gordonov, et al. Immunological Genome Consortium. 2012. Gene-expression profiles and transcriptional regulatory pathways that underlie the identity and diversity of mouse tissue macrophages. *Nat. Immunol.* 13:1118–1128. https://doi.org/10.1038/ni.2419

Ginhoux, F., and S. Jung. 2014. Monocytes and macrophages: developmental pathways and tissue homeostasis. *Nat. Rev. Immunol.* 14:392–404. https://doi.org/10.1038/nri3671

Ginhoux, F., M. Greter, M. Leboeuf, S. Nandi, P. See, S. Gokhan, M.F. Mehler, S.J. Conway, L.G. Ng, E.R. Stanley, et al. 2010. Fate mapping analysis reveals that adult microglia derive from primitive macrophages. *Science.* 330:841–845. https://doi.org/10.1126/science.1194637

Gordon, S. 2003. Alternative activation of macrophages. *Nat. Rev. Immunol.* 3:23–35. https://doi.org/10.1038/nri978

Huang, S.C., B. Everts, Y. Ivanova, D. O'Sullivan, M. Nascimento, A.M. Smith, W. Beatty, L. Love-Gregory, W.Y. Lam, C.M. O'Neill, et al. 2014. Cell-intrinsic lysosomal lipolysis is essential for alternative activation of macrophages. *Nat. Immunol.* 15:846–855. https://doi.org/10.1038/ni.2956

Hughes, J.E., S. Srinivasan, K.R. Lynch, R.L. Proia, P. Ferdek, and C.C. Hedrick. 2008. Sphingosine-1-phosphate induces an antiinflammatory phenotype in macrophages. *Circ. Res.* 102:950–958. https://doi.org/10.1161/CIRCRESAHA.107.170779

Inbar, E., N.S. Akopyants, M. Charmoy, A. Romano, P. Lawyer, D.E. Elnaiem, F. Kauffmann, M. Barhoumi, M. Grigg, K. Owens, et al. 2013. The mating competence of geographically diverse Leishmania major strains in their natural and unnatural sand fly vectors. *PLoS Genet.* 9:e1003672. https://doi.org/10.1371/journal.pgen.1003672

Jakubzick, C., E.L. Gautier, S.L. Gibbings, D.K. Sojka, A. Schlitzer, T.E. Johnson, S. Ivanov, Q. Duan, S. Bala, T. Condon, et al. 2013. Minimal differentiation of classical monocytes as they survey steady-state tissues and transport antigen to lymph nodes. *Immunity.* 39:599–610. https://doi.org/10.1016/j.immuni.2013.08.007

Jenkins, S.J., D. Ruckerl, P.C. Cook, L.H. Jones, F.D. Finkelman, N. van Rooijen, A.S. MacDonald, and J.E. Allen. 2011. Local macrophage proliferation, rather than recruitment from the blood, is a signature of TH2 inflammation. *Science.* 332:1284–1288. https://doi.org/10.1126/science.1204351

Kostka, S.L., J. Knop, A. Konur, M.C. Udey, and E. von Stebut. 2006. Distinct roles for IL-1 receptor type I signaling in early versus established Leishmania major infections. *J. Invest. Dermatol.* 126:1582–1589. https://doi.org/10.1038/sj.jid.5700309

Lavin, Y., D. Winter, R. Blecher-Gonen, E. David, H. Keren-Shaul, M. Merad, S. Jung, and I. Amit. 2014. Tissue-resident macrophage enhancer landscapes are shaped by the local microenvironment. *Cell.* 159:1312–1326. https://doi.org/10.1016/j.cell.2014.11.018

Lazarski, C.A., J. Ford, S.D. Katzman, A.F. Rosenberg, and D.J. Fowell. 2013. IL-4 attenuates Th1-associated chemokine expression and Th1 trafficking to inflamed tissues and limits pathogen clearance. *PLoS One.* 8:e71949. https://doi.org/10.1371/journal.pone.0071949

Lee, S.J., S. Evers, D. Roeder, A.F. Parlow, J. Risteli, L. Risteli, Y.C. Lee, T. Feizi, H. Langen, and M.C. Nussenzweig. 2002. Mannose receptor-mediated regulation of serum glycoprotein homeostasis. *Science.* 295:1898–1901. https://doi.org/10.1126/science.1069540

Linehan, S.A., L. Martínez-Pomares, and S. Gordon. 2000. Macrophage lectins in host defence. *Microbes Infect.* 2:279–288. https://doi.org/10.1016/S1286-4579(00)00300-2

Louzir, H., P.C. Melby, A. Ben Salah, H. Marrakchi, K. Aoun, R. Ben Ismail, and K. Dellagi. 1998. Immunologic determinants of disease evolution in

localized cutaneous leishmaniasis due to Leishmania major. *J. Infect. Dis.* 177:1687–1695. https://doi.org/10.1086/515297

MacDonald, K.P., J.S. Palmer, S. Cronau, E. Seppanen, S. Olver, N.C. Raffelt, R. Kuns, A.R. Pettit, A. Clouston, B. Wainwright, et al. 2010. An antibody against the colony-stimulating factor 1 receptor depletes the resident subset of monocytes and tissue- and tumor-associated macrophages but does not inhibit inflammation. *Blood*. 116:3955–3963. https://doi.org/10.1182/blood-2010-02-266296

Martinez-Pomares, L., D.M. Reid, G.D. Brown, P.R. Taylor, R.J. Stillion, S.A. Linehan, S. Zamze, S. Gordon, and S.Y. Wong. 2003. Analysis of mannose receptor regulation by IL-4, IL-10, and proteolytic processing using novel monoclonal antibodies. *J. Leukoc. Biol.* 73:604–613. https://doi.org/10.1189/jlb.0902450

Murray, P.J. 2017. Macrophage Polarization. *Annu. Rev. Physiol.* 79:541–566. https://doi.org/10.1146/annurev-physiol-022516-034339

Murray, P.J., J.E. Allen, S.K. Biswas, E.A. Fisher, D.W. Gilroy, S. Goerdt, S. Gordon, J.A. Hamilton, L.B. Ivashkiv, T. Lawrence, et al. 2014. Macrophage activation and polarization: nomenclature and experimental guidelines. *Immunity.* 41:14–20. https://doi.org/10.1016/j.immuni.2014.06.008

Neva, F.A., D. Wyler, and T. Nash. 1979. Cutaneous leishmaniasis--a case with persistent organisms after treatment in presence of normal immune response. *Am. J. Trop. Med. Hyg.* 28:467–471. https://doi.org/10.4269/ajtmh.1979.28.467

Pirmez, C., M. Yamamura, K. Uyemura, M. Paes-Oliveira, F. Conceição-Silva, and R.L. Modlin. 1993. Cytokine patterns in the pathogenesis of human leishmaniasis. *J. Clin. Invest.* 91:1390–1395. https://doi.org/10.1172/JCI116341

Pyonteck, S.M., L. Akkari, A.J. Schuhmacher, R.L. Bowman, L. Sevenich, D.F. Quail, O.C. Olson, M.L. Quick, J.T. Huse, V. Teijeiro, et al. 2013. CSF-1R inhibition alters macrophage polarization and blocks glioma progression. *Nat. Med.* 19:1264–1272. https://doi.org/10.1038/nm.3337

Qualls, J.E., G. Neale, A.M. Smith, M.S. Koo, A.A. DeFreitas, H. Zhang, G. Kaplan, S.S. Watowich, and P.J. Murray. 2010. Arginine usage in mycobacteria-infected macrophages depends on autocrine-paracrine cytokine signaling. *Sci. Signal.* 3:ra62. https://doi.org/10.1126/scisignal.2000955

Rothenberg, M.E., and S.P. Hogan. 2006. The eosinophil. *Annu. Rev. Immunol.* 24:147–174. https://doi.org/10.1146/annurev.immunol.24.021605.090720

Rückerl, D., S.M. Campbell, S. Duncan, T.E. Sutherland, S.J. Jenkins, J.P. Hewitson, T.A. Barr, L.H. Jackson-Jones, R.M. Maizels, and J.E. Allen. 2017. Macrophage origin limits functional plasticity in helminth-bacterial co-infection. *PLoS Pathog.* 13:e1006233. https://doi.org/10.1371/journal.ppat.1006233

Sacks, D.L., and R.P. da Silva. 1987. The generation of infective stage Leishmania major promastigotes is associated with the cell-surface expression and release of a developmentally regulated glycolipid. *J. Immunol.* 139:3099–3106.

Santarlasci, V., L. Cosmi, L. Maggi, F. Liotta, and F. Annunziato. 2013. IL-1 and T Helper Immune Responses. *Front. Immunol.* 4:182. https://doi.org/10.3389/fimmu.2013.00182

Sauter, K.A., C. Pridans, A. Sehgal, Y.T. Tsai, B.M. Bradford, S. Raza, L. Moffat, D.J. Gow, P.M. Beard, N.A. Mabbott, et al. 2014. Pleiotropic effects of extended blockade of CSF1R signaling in adult mice. *J. Leukoc. Biol.* 96:265–274. https://doi.org/10.1189/jlb.2A0114-006R

Schleicher, U., K. Paduch, A. Debus, S. Obermeyer, T. König, J.C. Kling, E. Ribechini, D. Dudziak, D. Mougiakakos, P.J. Murray, et al. 2016. TNF-Mediated Restriction of Arginase 1 Expression in Myeloid Cells Triggers Type 2 NO Synthase Activity at the Site of Infection. *Cell Reports.* 15:1062–1075. https://doi.org/10.1016/j.celrep.2016.04.001

Schlesinger, L.S. 1993. Macrophage phagocytosis of virulent but not attenuated strains of Mycobacterium tuberculosis is mediated by mannose receptors in addition to complement receptors. *J. Immunol.* 150:2920–2930.

Schreiber, S., S.L. Perkins, S.L. Teitelbaum, J. Chappel, P.D. Stahl, and J.S. Blum. 1993. Regulation of mouse bone marrow macrophage mannose receptor expression and activation by prostaglandin E and IFN-gamma. *J. Immunol.* 151:4973–4981.

Shaul, M.E., G. Bennett, K.J. Strissel, A.S. Greenberg, and M.S. Obin. 2010. Dynamic, M2-like remodeling phenotypes of CD11c+ adipose tissue macrophages during high-fat diet--induced obesity in mice. *Diabetes.* 59:1171–1181. https://doi.org/10.2337/db09-1402

Späth, G.F., and S.M. Beverley. 2001. A lipophosphoglycan-independent method for isolation of infective Leishmania metacyclic promastigotes by density gradient centrifugation. *Exp. Parasitol.* 99:97–103. https://doi.org/10.1006/expr.2001.4656

Stein, M., S. Keshav, N. Harris, and S. Gordon. 1992. Interleukin 4 potently enhances murine macrophage mannose receptor activity: a marker of alternative immunologic macrophage activation. *J. Exp. Med.* 176:287–292. https://doi.org/10.1084/jem.176.1.287

Stenger, S., N. Donhauser, H. Thüring, M. Röllinghoff, and C. Bogdan. 1996. Reactivation of latent leishmaniasis by inhibition of inducible nitric oxide synthase. *J. Exp. Med.* 183:1501–1514. https://doi.org/10.1084/jem.183.4.1501

Tamoutounour, S., M. Guilliams, F. Montanana Sanchis, H. Liu, D. Terhorst, C. Malosse, E. Pollet, L. Ardouin, H. Luche, C. Sanchez, et al. 2013. Origins and functional specialization of macrophages and of conventional and monocyte-derived dendritic cells in mouse skin. *Immunity.* 39:925–938. https://doi.org/10.1016/j.immuni.2013.10.004

Thornley, T.B., Z. Fang, S. Balasubramanian, R.A. Larocca, W. Gong, S. Gupta, E. Csizmadia, N. Degauque, B.S. Kim, M. Koulmanda, et al. 2014. Fragile TIM-4-expressing tissue resident macrophages are migratory and immunoregulatory. *J. Clin. Invest.* 124:3443–3454. https://doi.org/10.1172/JCI73527

Ueno, N., and M.E. Wilson. 2012. Receptor-mediated phagocytosis of Leishmania: implications for intracellular survival. *Trends Parasitol.* 28:335–344. https://doi.org/10.1016/j.pt.2012.05.002

Wei, X.Q., I.G. Charles, A. Smith, J. Ure, G.J. Feng, F.P. Huang, D. Xu, W. Muller, S. Moncada, and F.Y. Liew. 1995. Altered immune responses in mice lacking inducible nitric oxide synthase. *Nature.* 375:408–411. https://doi.org/10.1038/375408a0

Wollenberg, A., M. Mommaas, T. Oppel, E.M. Schottdorf, S. Günther, and M. Moderer. 2002. Expression and function of the mannose receptor CD206 on epidermal dendritic cells in inflammatory skin diseases. *J. Invest. Dermatol.* 118:327–334. https://doi.org/10.1046/j.0022-202x.2001.01665.x

Wright, D.E., A.J. Wagers, A.P. Gulati, F.L. Johnson, and I.L. Weissman. 2001. Physiological migration of hematopoietic stem and progenitor cells. *Science.* 294:1933–1936. https://doi.org/10.1126/science.1064081

Yona, S., K.W. Kim, Y. Wolf, A. Mildner, D. Varol, M. Breker, D. Strauss-Ayali, S. Viukov, M. Guilliams, A. Misharin, et al. 2013. Fate mapping reveals origins and dynamics of monocytes and tissue macrophages under homeostasis. *Immunity.* 38:79–91. https://doi.org/10.1016/j.immuni.2012.12.001

Zagórska, A., P.G. Través, E.D. Lew, I. Dransfield, and G. Lemke. 2014. Diversification of TAM receptor tyrosine kinase function. *Nat. Immunol.* 15:920–928. https://doi.org/10.1038/ni.2986